THE JOURNAL OF BIOLOGICAL CHEMISTRY VOL. 290, NO. 5, pp. 2854–2869, January 30, 2015

Functional Characterization of $Ca_V\alpha2\delta$ Mutations Associated with Sudden Cardiac Death*

Received for publication, July 18, 2014, and in revised form, December 12, 2014 Published, JBC Papers in Press, December 19, 2014, DOI 10.1074/jbc.M114.597930

Benoîte Bourdin[‡1], **Behzad Shakeri**[‡1], **Marie-Philippe Tétreault**[‡], **Rémy Sauvé**[‡], **Sylvie Lesage**[§], **and Lucie Parent**[‡2]

From the [‡]*Département de Physiologie, Montreal Heart Institute Research Centre, and* [§]*Département de Microbiologie, Infectiologie et Immunologie, Centre de Recherche de l'Hôpital Maisonneuve-Rosemont, Université de Montréal, Montréal, Québec H3C 3J7, Canada*

Background: Missense mutations in $Ca_V\alpha2\delta1$, an auxiliary subunit of cardiac L-type $Ca_V1.2$ channels, are associated with arrhythmias.
Results: The reduction in the cell surface density of $Ca_V\alpha2\delta1$ D550Y/Q917H was sufficient to impair $Ca_V1.2$ currents.
Conclusion: Defects in the cell surface trafficking of $Ca_V\alpha2\delta1$ mutants down-regulate L-type currents.
Significance: *CACNA2D1* genetic variants may trigger arrhythmias by reducing L-type Ca^{2+} currents.

L-type Ca^{2+} channels play a critical role in cardiac rhythmicity. These ion channels are oligomeric complexes formed by the pore-forming $Ca_V\alpha1$ with the auxiliary $Ca_V\beta$ and $Ca_V\alpha2\delta$ subunits. $Ca_V\alpha2\delta$ increases the peak current density and improves the voltage-dependent activation gating of $Ca_V1.2$ channels without increasing the surface expression of the $Ca_V\alpha1$ subunit. The functional impact of genetic variants of *CACNA2D1* (the gene encoding for $Ca_V\alpha2\delta$), associated with shorter repolarization QT intervals (the time interval between the Q and the T waves on the cardiac electrocardiogram), was investigated after recombinant expression of the full complement of L-type $Ca_V1.2$ subunits in human embryonic kidney 293 cells. By performing side-by-side high resolution flow cytometry assays and whole-cell patch clamp recordings, we revealed that the surface density of the $Ca_V\alpha2\delta$ wild-type protein correlates with the peak current density. Furthermore, the cell surface density of $Ca_V\alpha2\delta$ mutants S755T, Q917H, and S956T was not significantly different from the cell surface density of the $Ca_V\alpha2\delta$ wild-type protein expressed under the same conditions. In contrast, the cell surface expression of $Ca_V\alpha2\delta$ D550Y, $Ca_V\alpha2\delta$ S709N, and the double mutant D550Y/Q917H was reduced, respectively, by ≈30–33% for the single mutants and by 60% for the latter. The cell surface density of D550Y/Q917H was more significantly impaired than protein stability, suggesting that surface trafficking of $Ca_V\alpha2\delta$ was disrupted by the double mutation. Co-expression with D550Y/Q917H significantly decreased $Ca_V1.2$ currents as compared with results obtained with $Ca_V\alpha2\delta$ wild type. It is concluded that D550Y/Q917H reduced inward Ca^{2+} currents through a defect in the cell surface trafficking of $Ca_V\alpha2\delta$. Altogether, our results provide novel insight in the molecular mechanism underlying the modulation of $Ca_V1.2$ currents by $Ca_V\alpha2\delta$.

Polymorphic ventricular tachycardia is one of the leading causes of sudden cardiac death in children and young adults (1). These cardiac arrhythmias, which are reported in the absence of structural heart defects, coronary artery disease, or heart failure, are detected in a noninvasive fashion by measuring changes in the QT[3] interval on the electrocardiogram. Either excessive prolongation (LQT) or shortening of the QT (SQT) intervals are associated with an increased risk of sudden cardiac death (2). Inherited Mendelian long QT syndrome (LQTS) and short QT syndrome (SQTS) originate from mutations in genes encoding ion channels or channel-interacting proteins (3). Genome-wide linkage studies of families with LQTS have reported 13 LQTS susceptibility genes with 75% of LQTS cases stemming from mutations in *KCNQ1* (LQT1), *KCNH2* (LQT2), and *SCN5A* (LQT3) (4). Only recently have mutations of genes coding for subunits forming the L-type Ca^{2+} channel been linked to inherited arrhythmogenic diseases caused by LQTS or SQTS (5). The molecular mechanism underlying the cardiac dysfunction remains unknown in many cases.

The *CACNA1C* gene encodes the L-type $Ca_V1.2$ channel that carries the vast majority of the L-type calcium current in the adult heart (6, 7) which in turn initiates the coordinated contraction of the cardiac ventricles (8). Its unique role is substantiated by the observation that homozygous knock-out of the *CACNA1C* gene is lethal (9, 10). In addition to initiating the coordinated contraction of the cardiac ventricles, $Ca_V1.2$ channels are critical to the heart's normal rhythmic activity (8). During the cardiac action potential, Ca^{2+} enters the cell through the voltage-dependent L-type $Ca_V1.2$ generating an inward Ca^{2+} current that contributes to the plateau phase of the action potential (11). The kinetic properties of this channel must be properly timed so that depolarization and contraction are synchronized during the systolic-diastolic cycle of the heart. Even a slight disruption of Ca^{2+} cycling can have a profound impact on action-potential duration and trigger early after depolarizations, ultimately cumulating in lethal

* This work was supported by Operating Grant 130256 from the Canadian Institutes of Health Research and a grant from the Canadian Heart and Stroke Foundation (to L. P.).
[1] Both authors contributed equally to this work.
[2] To whom correspondence should be addressed: Dept. of Physiology, Université de Montréal, P. O. Box 6128, Downtown Station, Montréal, Quebec H3C 3J7, Canada. Tel.: 514-343-6673; E-mail: lucie.parent@umontreal.ca.

[3] The abbreviations used are: QT, time interval between the Q and the T waves on the cardiac electrocardiogram; HEKT, human embryonic kidney 293 cell; LQTS, long QT syndrome; MFI, mean fluorescent intensity; SQTS, short QT syndrome; pF, picofarad.

arrhythmias (5, 12), including torsade de pointes and ventricular fibrillation (2). Prolonged inward Ca^{2+} current during the plateau phase of the cardiac action potential leads to delays in ventricular myocyte repolarization, a subsequent prolonged QT repolarization interval on the electrocardiogram and a highly arrhythmogenic and potentially lethal substrate. On the other end of the spectrum, any significant decrease in inward currents or significant increase in outward currents may lead to lethal arrhythmias associated with shorter than normal QT repolarization intervals (3).

The L-type $Ca_V1.2$ channel belongs to the molecular family of high voltage activated Ca_V channels. High voltage-activated $Ca_V1.2$ channels are hetero-oligomers formed by the main pore-forming $Ca_V\alpha1$ subunit in a complex with the cytoplasmic $Ca_V\beta$ auxiliary subunit, the EF-hand protein calmodulin constitutively bound to the C terminus of $Ca_V\alpha1$, and the mostly extracellular $Ca_V\alpha2\delta$ subunit (13–18). The full complement of auxiliary subunits is required to produce high voltage-activated $Ca_V1.2$ channels with the properties of the native channels. $Ca_V\beta$ promotes the cell surface density of $Ca_V1.2$ channels (19) in part by preventing its degradation by the ubiquitin/proteasome system (20). Co-expression of $Ca_V\alpha2\delta$ subunit with $Ca_V\beta$-bound $Ca_V\alpha1$ increases peak current density and hyperpolarizes the voltage of activation of the L-type $Ca_V1.2$ (19, 21–23).

Gain-of-function mutations in the pore-forming $Ca_V\alpha1$ subunit of the L-type Ca^{2+} channel lead to the highly arrhythmogenic Timothy syndrome. Timothy syndromes 1 and 2 are rare variants of the long QT syndrome (LQT8) (24, 25) characterized by extreme QT-prolongation and gain-of-function mutations in the pore-forming subunit of $Ca_V1.2$ (24–28). Mutations in the auxiliary subunits forming the L-type $Ca_V1.2$ channel have also been identified among probands diagnosed with Brugada syndrome, idiopathic ventricular fibrillation, and early repolarization syndrome associated with short QT interval (QTc ≤360 ms) (29–31). According to these studies, the shorter QT interval might result from loss-of-function mutations in the Ca_V genes coding for $Ca_V\alpha1$ (*CACNA1C*), $Ca_V\beta$ (*CACNB2*), or $Ca_V\alpha2\delta$ (*CACNA2D1*). Missense mutations D550Y, S709N, S755T, Q917H, and S956T in the $Ca_V\alpha2\delta1$ protein have been associated with congenital arrhythmias (referred to as short QT syndrome 6 (SQT6) (29–31)), but the molecular mechanism(s) underlying the change in function remains to be established (32).

In this work, we have characterized the $Ca_V\alpha2\delta$ mutations associated with arrhythmogenic activity in regard to their functional impact on the cardiac L-type $Ca_V1.2$ currents. Using a fluorescence-labeled and extracellularly tagged $Ca_V\alpha2\delta$ subunit, we show here that missense mutations D550Y, S709N and D550Y/Q917H significantly altered the cell surface density of $Ca_V\alpha2\delta$. Decreasing the cell surface density of $Ca_V\alpha2\delta$ D550Y/Q917H was found to profoundly decrease L-type peak current densities as compared with currents measured with $Ca_V\alpha2\delta$ wild type (WT). Altogether, our data support a model where $Ca_V\alpha2\delta$ modulates channel function without altering the trafficking of $Ca_V1.2$ and establishes the cell surface density of $Ca_V\alpha2\delta$ relative to the pore-forming $Ca_V\alpha1$ as the single most important determinant in the stimulation of $Ca_V1.2$ currents by $Ca_V\alpha2\delta$.

EXPERIMENTAL PROCEDURES

Recombinant DNA Techniques—The rabbit $Ca_V1.2$ (GenBank™ X15539), the rat $Ca_V\beta3$ (GenBank™ M88751) (33), and the rat brain $Ca_V\alpha2\delta1$ (GenBank™ NM_012919) (34) were subcloned in commercial vectors under the control of the CMV promoter as described elsewhere (19, 35). The primary sequence of the rat brain $Ca_V\alpha2\delta1$ clone (1091 residues) is 96% identical to the predicted sequence of the human clone NM_000722 (1091 residues). All residues mutated in the following experiments are conserved between species. The first series of experiments (Figs. 1 and 2) was conducted with a tagged version of $Ca_V1.2$ whereby the hemagglutinin (HA) epitope (YPYDVPDYA) was inserted in the extracytoplasmic loop of $Ca_V1.2$ in the S5-S6 linker of domain II between residues 710 and 711, whereas the untagged version of $Ca_V1.2$ was used in the experiments shown in Figs. 3–11. The rat $Ca_V\alpha2\delta1$ was subcloned in the pmCherry-N1 vector (Cederlane, Burlington, Ontario, Canada) between the SacI and SalI sites. In this construct, the hemagglutinin (HA) epitope (YPYDVPDYA) was inserted in the extracellular domain of $Ca_V\alpha2$. More than 10 different insertion sites were tested in $Ca_V\alpha2$, but only one was found to be functional and fluorescently labeled with a FITC-labeled anti-HA (fluorescein isothiocyanate) (results not shown). The insertion site was identified at position Arg-676 in the extracellular domain. Cell surface and total density of $Ca_V\alpha2\delta$ were evaluated by two-color flow cytometry assays using the pmCherry-$Ca_V\alpha2\delta1$-HA construct. Unless specified otherwise, the flow cytometry experiments and the patch clamp recordings were systematically conducted with this pmCherry-$Ca_V\alpha2\delta$-1-HA construct.

Site-directed Mutagenesis—All mutants were produced with the Q5 site-directed mutagenesis kit (New England Biolabs, Whitby, Ontario, Canada) according to the manufacturer's instructions. Briefly, amino acid substitutions were performed by nonoverlapping desalted primers. Substitutions are created by incorporating the desired mutation in the center of the forward primer, and the reverse primer is designed so that the 5′ ends of the two primers anneal back-to-back. Following the PCR, a kinase/ligase/DpnI enzyme mixture was added to the amplified DNA for circularization and template removal before transformation into high efficiency DH5α-competent *Escherichia coli*. Constructs were verified by automated double-stranded sequence analysis (Genomics Platform, IRIC, Université de Montréal, Quebec, Canada). Protein expression of all constructs was confirmed by Western blotting in total cell lysates as described previously (19).

Cell Culture and Transfections—HEK293T or HEKT cells were grown in Dulbecco's high glucose minimum essential medium (DMEM-HG) supplemented with 10% fetal bovine serum, 1% penicillin/streptomycin at 37 °C under 5% CO_2 atmosphere as described elsewhere (19). RT-PCR conducted in these cells failed to highlight the presence of $Ca_V\beta$ and $Ca_V\alpha2\delta$ auxiliary subunits (36). All experiments described herein were conducted in HEKT cells stably transfected with $Ca_V\beta3$, as this isoform was best at promoting the cell surface density of $Ca_V1.2$ (19). The use of stable cells limited the problems linked to protein overexpression. Unless specified otherwise, stable $Ca_V\beta3$

cells (90% confluence) were transiently transfected with similar amounts of DNA (4 μg each for a total of 8 μg total per 10^6 cells) as follows: $Ca_V1.2$ WT-HA (Figs. 1 and 2), $Ca_V1.2$ WT (Figs. 3–11), $Ca_V\alpha2\delta1$ WT, $Ca_V\alpha2\delta1$-HA, or empty vector in 10 μl of Lipofectamine 2000 (Invitrogen) using a DNA/lipid ratio of 1:2.5 as described elsewhere (19). In some experiments, the amount of DNA for $Ca_V\alpha2\delta$ was decreased in the 0.2–4.0-μg range to decrease the $Ca_V\alpha2\delta/Ca_V1.2$ expression ratio, but the total DNA amount was kept constant at 8 μg by using a mock vector.

Antibodies and Reagents—The following primary antibodies were used for Western blots: anti-$Ca_V1.2$ (Alomone Labs, Jerusalem, Israel) (1:5000); anti-$Ca_V\alpha2\delta$ (Alomone Labs) (1:500); anti-$Ca_V\beta3$ (Alomone Labs) (1:5000); anti-mCherry (Biovision, Milpitas, CA) (1:20,000); anti-HA (Covance Biotechnology, Quebec, Canada) (1:1000); and anti-GAPDH (Sigma) (1:10,000). Cycloheximide was used at 100 μg/ml for up to 48 h (Sigma). For the flow cytometry assays, the HA tag was detected using the FITC-conjugated mouse monoclonal anti-HA (Sigma) (5 μg/ml). We used the mouse IgG1 isotype control antibody conjugated to FITC (Sigma) to help assess the level of background staining in the flow cytometry experiments (5 μg/ml).

Flow Cytometry Experiments—Flow cytometry experiments were conducted as described elsewhere (19, 35). To determine the cell surface expression level of the tagged proteins, cells were harvested 24 h after transfection, washed in a PBS 1× buffer, and stained with the FITC-labeled anti-HA epitope tag antibody at 5 μg/ml (Clone HA-7, Sigma) at 4 °C for 30 min. To determine the density of both intracellular and extracellular expression of the tagged proteins, cells were fixed and permeabilized using BD Cytofix/Cytoperm™ fixation/permeabilization solution kit (BD Biosciences, 554714) according to the manufacturer's instructions. Briefly, cells were washed with the 1× BD Perm/Wash buffer containing both FBS and saponin and stained 30 min at 4 °C with the FITC-labeled anti-HA epitope tag antibody. A maximum of 10,000 cells were counted using a FACSAria III® special order research product flow cytometer (BD Biosciences) at the flow cytometry facility located at the Department of Microbiology, Université de Montréal. Relative expression of $Ca_V\alpha2\delta$ was calculated based on Δmean fluorescence intensity (ΔMFI) for each fluorophore (mCherry or FITC) rather than computing the number of fluorescent cells (see below) (19). Three control conditions were always carried out for each series of experiments as follows: (*a*) untransfected HEKT cells with the murine IgG1-FITC isotype control (5 μg/ml); (*b*) transfected HEKT cells without the anti-HA FITC antibody but with the murine IgG1-FITC isotype control (5 μg/ml); (*c*) HEKT cells transfected with the wild-type HA-tagged construct. No fluorescence was detected with the IgG1-FITC isotype control murine (5 μg/ml) nor in untransfected cells with the anti-HA FITC conjugated antibody (5 μg/ml) (data not shown). The fluorescence intensity of each construct transfected in any given condition was measured using six distinct cell dishes for an average of 60,000 cells for each condition. Flow cytometry experiments performed at 36 h to mimic as closely as possible the experimental conditions used for the patch clamp experiments (see below), yielded quantitatively similar results as experiments performed at 24 h (data not shown).

Quantification of Cell Surface Expression—Flow cytometry data were analyzed, and figures were produced using the FlowJo software, version 10 (TreeStar, Ashland, OR). Dead cells were excluded based on forward scatter/side scatter profiles. The FITC-positive cells gate (P2) and the FITC negative cells gate (P3) were set manually. The FITC fluorescence intensity within the region delineated by the P2 and P3 gate was displayed as cell count *versus* FITC fluorescence intensity (*histograms* in Figs. 4, 5, and 8). The ΔMFI for FITC was calculated by subtracting the FITC fluorescence density of the FITC-negative cells (P3) from the fluorescence density of the FITC-positive cells (P2). ΔMFI was used as an index of the cell surface density of HA-tagged proteins (either HA-$Ca_V1.2$ or pmCherry-$Ca_V\alpha2\delta1$-HA) in intact nonpermeabilized cells or the total expression (cell surface and intracellular protein density) of HA-tagged proteins in permeabilized cells. The two HA-tagged proteins were never expressed together. Because cellular autofluorescence levels are altered by the change in the cell medium, the actual ΔMFI values in arbitrary units cannot be compared between intact nonpermeabilized and permeabilized cells. In Figs. 5 and 9, ΔMFI were pooled and normalized to the average value obtained for the pmCherry-$Ca_V\alpha2\delta1$-HA WT construct that was expressed under the same conditions and quantified under the same experimental conditions (see above).

Patch Clamp Experiments in HEKT Cells—Whole-cell voltage clamp recordings were performed on isolated cells 30–38 h after transfection using the methods described above in the presence of the peGFP vector (0.2 μg) as a control for transfection. In all cases, the experiments were carried out under optimal transfection conditions after assessment of the mCherry fluorescence of the mCherry-$Ca_V\alpha2\delta$ constructs. Patch clamp experiments were carried out with the Axopatch 200-B amplifier (Molecular Devices, Union City, CA). Electrodes were filled with a solution containing (in mM) 140 CsCl, 0.6 NaGTP, 3 MgATP, 10 EGTA, 10 HEPES, titrated to pH 7.3 with NaOH. Pipette resistance ranged from 2 to 4 megohms. Cells were bathed in a modified Earle's saline solution (in mM) as follows: 135 NaCl, 20 tetraethylammonium chloride, 2 $CaCl_2$, 1 $MgCl_2$, 10 HEPES, titrated to pH 7.3 with KOH. PClamp software Clampex 10.2 coupled to a Digidata 1440A acquisition system (Molecular Devices) was used for on-line data acquisition and analysis. Pipette and cell capacitance cancellation and series resistance compensation were applied (up to 80%) using the cancellation feature of the amplifier. Cellular capacitance was estimated by measuring the time constant of current decay evoked by a 10-mV depolarizing pulse applied to the cell from a holding potential of −100 mV. A series of 450-ms voltage pulses were applied from a holding potential of −100 mV at a frequency of 0.2 Hz, from −60 to +70 mV at 5-mV intervals. Unless stated otherwise, data were sampled at 5 kHz and filtered at 1 kHz. Experiments were performed at room temperature (20–22 °C). Activation parameters were estimated from the peak *I-V* curves obtained for each channel combination and are reported as the mean of individual measurements ± S.E. as described elsewhere (37). Briefly, the *I-V* relationships were normalized to the maximum amplitude and were fitted to a

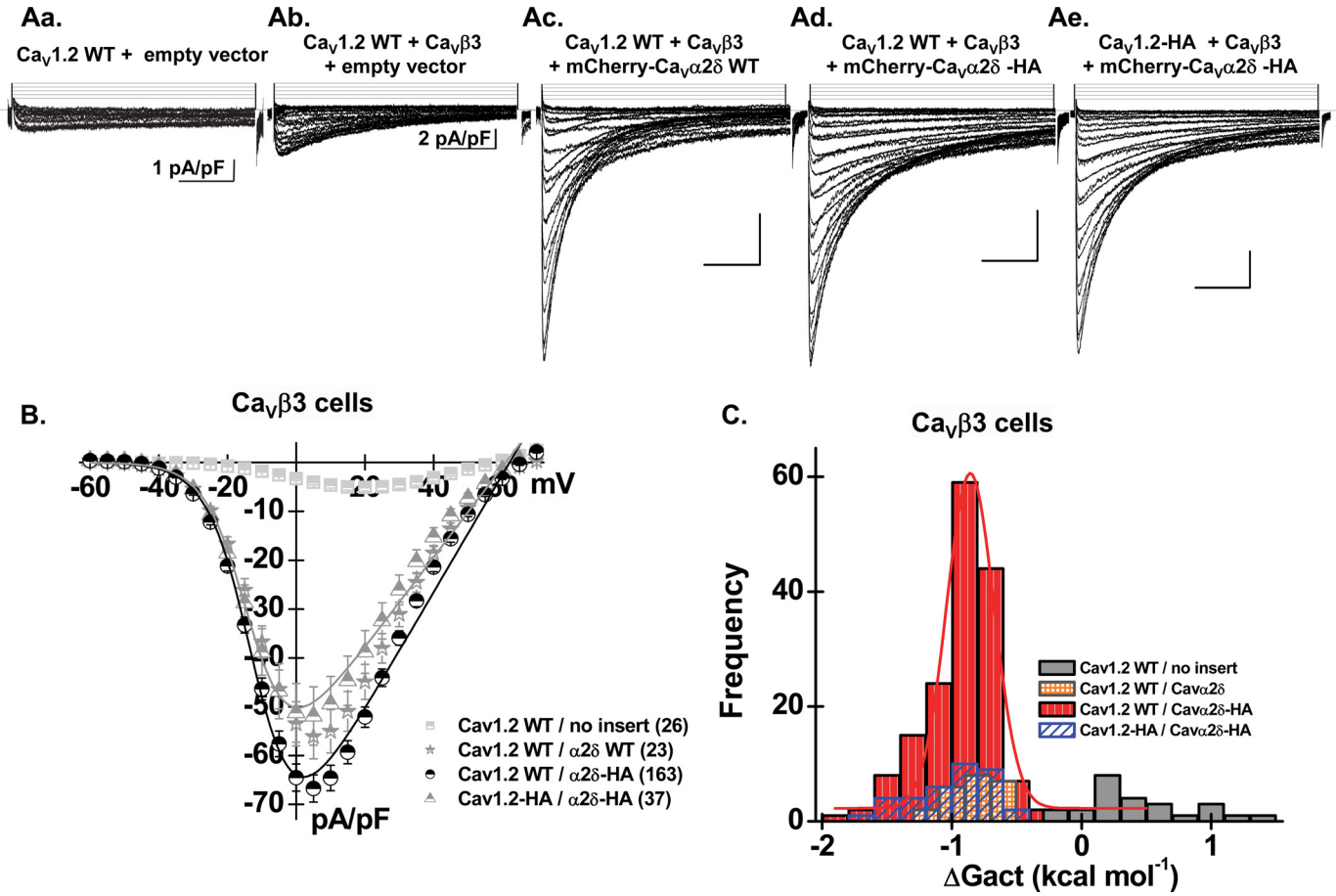

FIGURE 1. **$Ca_V\alpha2\delta1$ increases peak current density and hyperpolarizes the activation potential of $Ca_V1.2$.** *A*, pCMV-$Ca_V1.2$ (untagged version) was expressed in HEKT cells (*Aa*), in $Ca_V\beta3$ stable cells with an empty pCMV plasmid (*Ab*), in $Ca_V\beta3$ stable cells with pmCherry-$Ca_V\alpha2\delta1$ (*Ac*), and in $Ca_V\beta3$ stable cells with pmCherry-$Ca_V\alpha2\delta1$-HA (*Ad*). In addition, pCMV-$Ca_V1.2$-HA was expressed with pmCherry-$Ca_V\alpha2\delta1$-HA in $Ca_V\beta3$ stable cells in one series of experiments (*Ae*). Whole-cell current traces were recorded in the presence of 2 mM Ca^{2+} from a holding potential of −100 mV. Time scale is 100 ms throughout. Unless specified otherwise, the current density scale is 10 pA/pF. *B*, peak current densities increased from −5 ± 1 pA/pF (n = 26) for $Ca_V1.2$ WT/$Ca_V\beta3$ with an empty pmCherry vector to −56 ± 3 pA/pF (n = 23) in the presence of $Ca_V1.2$ WT/$Ca_V\beta3$ with pmCherry-$Ca_V\alpha2\delta1$ WT. Peak current densities measured in the presence of the following combinations were not statistically significantly different: $Ca_V1.2$ WT/$Ca_V\beta3$ with pmCherry-$Ca_V\alpha2\delta1$ WT; $Ca_V1.2$ WT/$Ca_V\beta3$ with pmCherry-$Ca_V\alpha2\delta1$-HA; and $Ca_V1.2$ HA/$Ca_V\beta3$ pmCherry-$Ca_V\alpha2\delta1$-HA. Co-expression with $Ca_V\alpha2\delta1$ WT shifted the voltage dependence of activation of $Ca_V1.2$ WT/$Ca_V\beta3$ from $E_{0.5,\,act}$ = 5 ± 2 mV (n = 26) (no $Ca_V\alpha2\delta$) to $E_{0.5,\,act}$ = −10.1 ± 0.5 mV (n = 23) (for $Ca_V1.2$ WT/$Ca_V\beta3$ with $Ca_V\alpha2\delta1$ WT), a significant −15 mV shift in the activation potential. The number in *parentheses* refers to the number of independent experiments. *C*, histogram is reporting the distribution of the individual ΔG_{act} values estimated in kilocalories/mol for each experimental condition (see "Experimental Procedures" for details). The ΔG_{act} values for $Ca_V1.2$ WT/$Ca_V\beta3$ with pmCherry-$Ca_V\alpha2\delta1$-HA were best fitted by a Gaussian equation with a σ = 0.36 centered around −0.86 kcal mol^{-1}. As seen, the distribution of the ΔG_{act} values measured in the absence of $Ca_V\alpha2\delta1$ subunit appeared to be flatter (varying from −0.1 to + 1.5 kcal mol^{-1}) and could not be properly fitted by a Gaussian equation.

Boltzmann equation with $E_{0.5,\,act}$ being the mid-potential of activation. The free energy of activation was calculated using the mid-activation potential shown in Equation 1,

$$\Delta G_{act} = z \cdot F \cdot E_{0.5,act} \qquad \text{(Eq. 1)}$$

where z is the effective charge displacement during activation, and F is the Faraday constant (38). The r100 ratio is defined as the ratio of peak whole-cell currents remaining after a depolarizing pulse of 100 ms ($I_{100\ ms}/I_{peak}$) and was used as an indicator of the inactivation kinetics.

Unless specified otherwise (as in Fig. 1), patch clamp experiments were performed with the untagged version of pCMV-$Ca_V1.2$ WT transfected with pmCherry-$Ca_V\alpha2\delta1$-HA WT or mutant in stable $Ca_V\beta3$ cells. Each novel pmCherry-$Ca_V\alpha2\delta1$-HA mutant was always tested alongside the control condition (pCMV-$Ca_V1.2$ WT + pmCherry-$Ca_V\alpha2\delta1$-HA WT in stable $Ca_V\beta3$ cells) to assess for internal consistency. Experiments performed under the same conditions yielded peak current densities ± 20% between samples and between series of experiments. All experiments were pooled and biophysical properties are reported in Table 1.

Statistics—Results were expressed as mean ± S.E. Tests of significance were carried out using the unpaired analysis of variance test embedded in the Origin 7.0 analysis software (OriginLab Corp., Northampton, MA). Data were considered statistically significant at $p < 0.05$.

RESULTS

HA-tagged $Ca_V\alpha2\delta$ Stimulates $Ca_V1.2$ Currents—Co-expression of $Ca_V1.2$ and $Ca_V2.2$ with the auxiliary $Ca_V\alpha2\delta$ subunit was shown to stimulate whole-cell currents (19, 39). Functional modulation of $Ca_V1.2$ by the various $Ca_V\alpha2\delta$ constructs was studied after recombinant expression in HEKT cell stably transfected with $Ca_V\beta3$ (Fig. 1*A*) as explained earlier (19). The immunoreactivity and the integrity of the constructs were verified by Western blotting (data not shown). As shown in Fig. 1*A*,

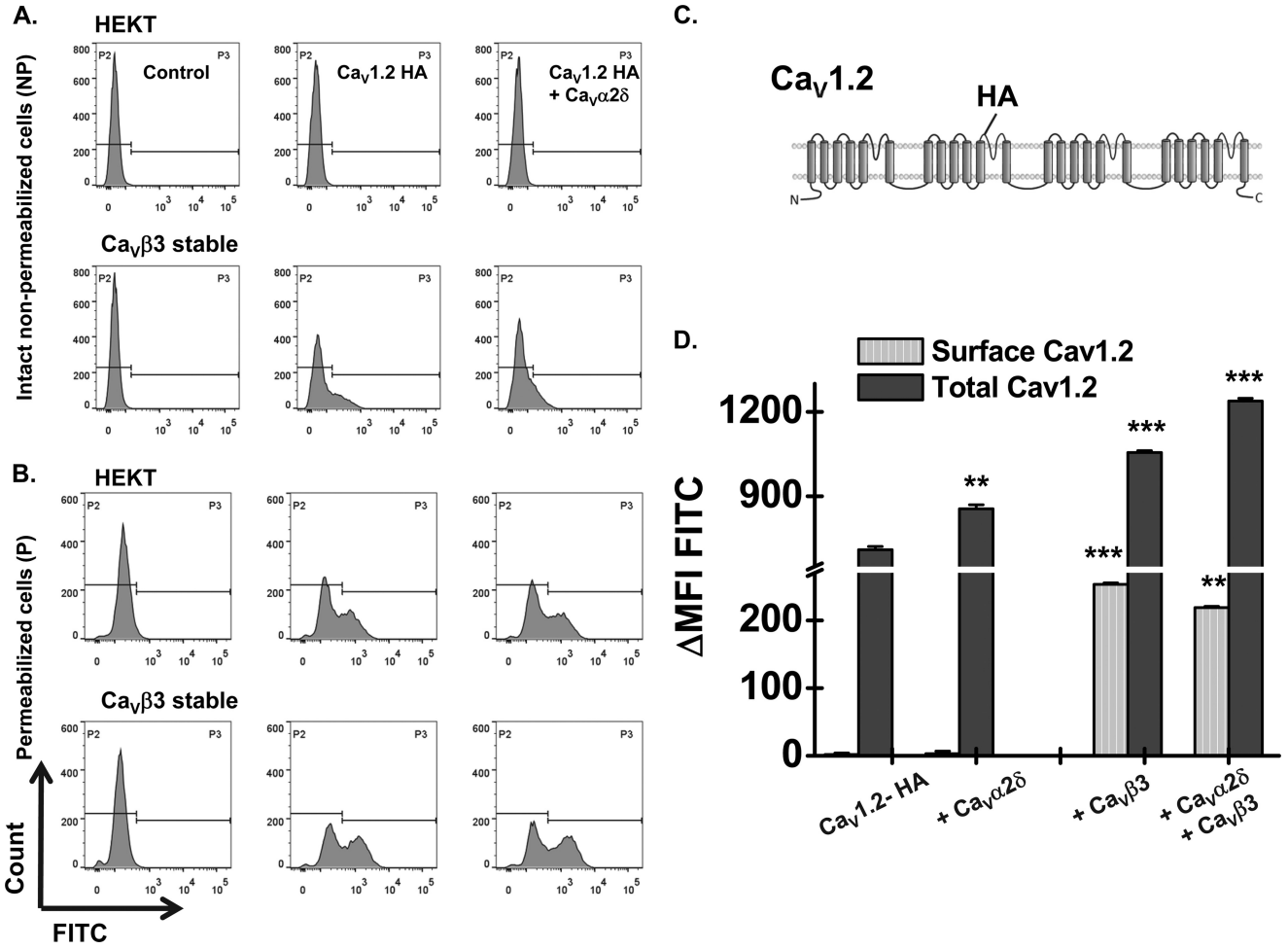

FIGURE 2. **Ca$_V$α2δ1 stimulates the total protein expression of Ca$_V$1.2 in HEKT cells.** HA-tagged Ca$_V$1.2 WT was co-expressed transiently either in HEKT cells (*A* and *B, top rows*) or in stable Ca$_V$β3 cells (*A* and *B, bottom rows*) with or without pCMV-Ca$_V$α2δ1. Cell surface expression of Ca$_V$1.2-HA WT was determined in intact nonpermeabilized cells (*A*) or after cell permeabilization by flow cytometry using the anti-HA FITC conjugate antibody (*B*). All histograms display live cells. ΔMFI was used as an index of the cell surface density of Ca$_V$1.2 in intact nonpermeabilized cells or the total expression (cell surface and intracellular protein density) of Ca$_V$1.2 in permeabilized cells. As seen, the surface expression of Ca$_V$1.2 was not significantly improved in the presence of Ca$_V$α2δ1 in contrast to the robust stimulation observed with Ca$_V$β3. The total protein expression of Ca$_V$1.2 was improved after co-expression with Ca$_V$α2δ1, but stronger stimulation was observed in the combined presence of Ca$_V$β3 with Ca$_V$α2δ1. *C,* predicted secondary structure of the HA-tagged Ca$_V$1.2 construct used in the figure. Please note that Ca$_V$α2δ1 was not tagged. *D, bar graph* summarizing the results shown in *A* and *B* with the values for the cell surface density in *light gray bars* and the total protein density in *dark gray bars*. Each experimental condition was quantified in triplicate. The fluorescence intensity is shown in arbitrary units. The statistical analysis was performed by comparing the ΔMFI values measured in all experimental groups *versus* ΔMFI values measured for Ca$_V$1.2-HA alone in intact *versus* permeabilized cells respectively. **, $p < 0.01$; ***, $p < 0.001$.

whole-cell currents, recorded in the presence of a saline solution containing a physiological concentration of Ca^{2+} (2 mM), were significantly larger when measured in the presence of the Ca$_V$α2δ confirming that Ca$_V$α2δ stimulates whole-cell currents of Ca$_V$1.2/Ca$_V$β3 (19). Peak current densities increased from -5 ± 1 pA/pF ($n = 26$) (no insert in the pmCherry vector) to -56 ± 3 pA/pF ($n = 23$) in the presence of Ca$_V$α2δ WT (Fig. 1*B*). The increase in peak current densities was associated with a −15-mV leftward shift in the activation potential of Ca$_V$1.2 from $E_{0.5,\,act} = 5 \pm 2$ mV ($n = 26$) (no Ca$_V$α2δ) to $E_{0.5,\,act} = -10.1 \pm 0.5$ mV ($n = 23$) (with Ca$_V$α2δ). Whole-cell currents recorded with untagged Ca$_V$1.2 WT + mCherry Ca$_V$α2δ-HA or with HA-tagged Ca$_V$1.2 + mCherry Ca$_V$α2δ-HA were not significantly different from currents recorded with untagged Ca$_V$1.2 WT + mCherry Ca$_V$α2δ WT. This result validates the constructions and confirms that the HA epitopes inserted in extracellular loops of both Ca$_V$α2δ and Ca$_V$1.2 are not occluding each other. The free energy of activation (ΔG_{act}) measured in the presence of Ca$_V$α2δ was well described by a Gaussian distribution centered around −0.86 kcal mol^{-1} (Fig. 1*C*), whereas the ΔG_{act} measured in the absence of Ca$_V$α2δ displayed a broader distribution centered at a value close to ≈0 kcal mol^{-1}. These results are compatible with a model whereby Ca$_V$α2δ stimulates peak current density by setting Ca$_V$1.2 channels in a conformational state very close to the open state (40).

*Ca$_V$α2δ Improves Total but Not Surface Expression of Ca$_V$1.2*—To evaluate the impact of Ca$_V$α2δ on the protein expression of Ca$_V$1.2, the HA-tagged version of Ca$_V$1.2 was expressed in HEKT cells and in stable Ca$_V$β3 cells in the presence or absence of Ca$_V$α2δ (Fig. 2). Flow cytometry assays were carried out in the presence of the FITC-conjugated anti-HA in intact and in permeabilized cells. Control experiments carried out with a pCMV-Ca$_V$1.2 control construct that was not HA-

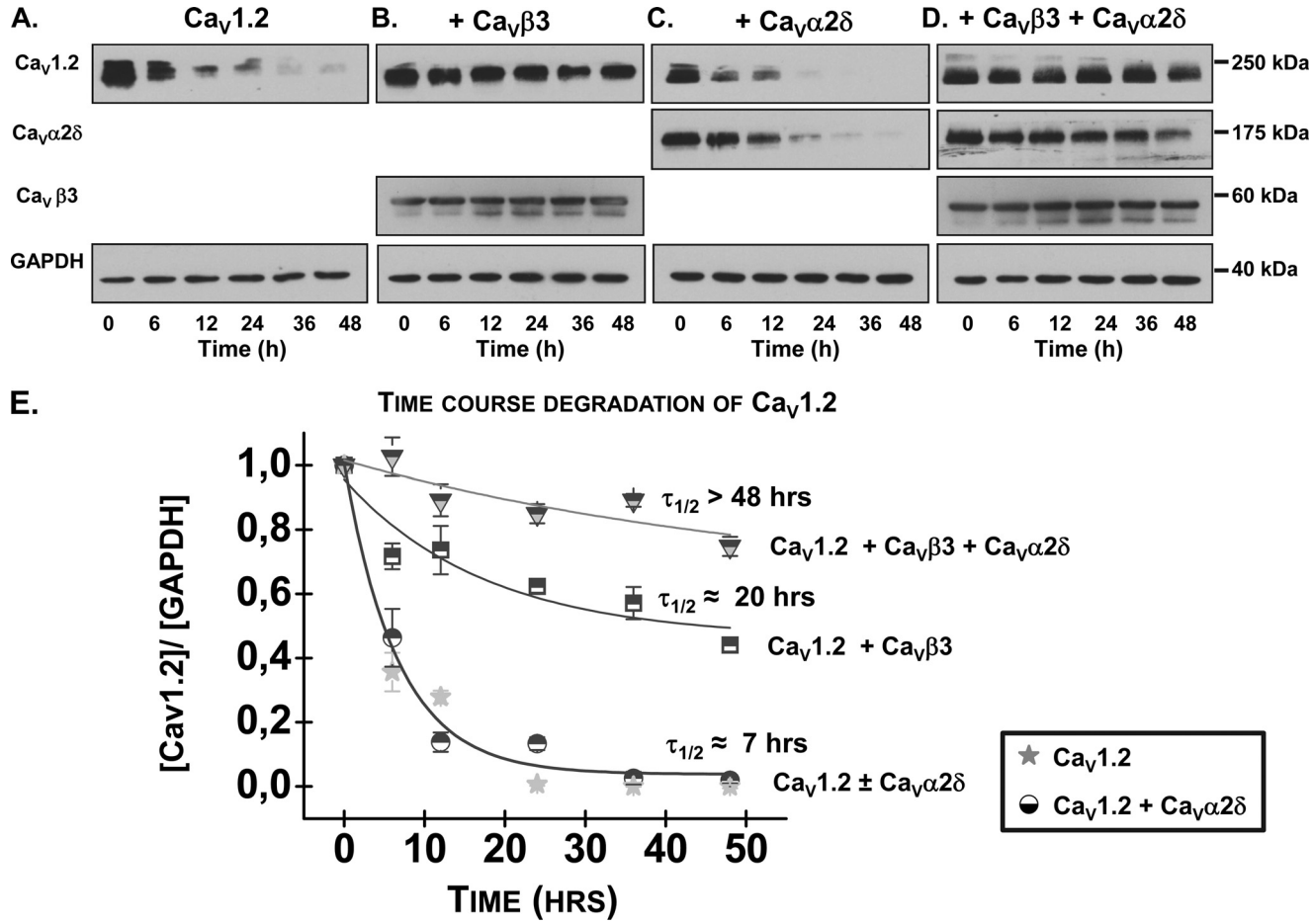

FIGURE 3. **Increased protein stability of the ternary complex $Ca_V1.2$-$Ca_V\beta$-$Ca_V\alpha2\delta1$ upon arrest of protein synthesis.** HEKT cells were transiently transfected simultaneously with the following constructions: *A,* pCMV-$Ca_V1.2$ and control plasmid; *B,* pCMV-$Ca_V1.2$ and pCMV-$Ca_V\beta3$; *C,* pCMV-$Ca_V1.2$ and pCMV-$Ca_V\alpha2\delta1$; and *D,* pCMV-$Ca_V1.2$, pCMV-$Ca_V\beta3$, and pCMV-$Ca_V\alpha2\delta1$. Exactly 24 h after transfection, subconfluent cells were incubated with cycloheximide (100 μg/ml) for up to 48 h to block *de novo* protein synthesis. At the indicated time points (0 h or no cycloheximide for 6, 12, 24, 36, and 48 h), cell lysates were prepared and fractionated by SDS-PAGE (10%), followed by immunoblotting to visualize $Ca_V1.2$, $Ca_V\beta3$, $Ca_V\alpha2\delta1$, and GAPDH. The protein density of $Ca_V1.2$ in total lysates was expressed relative to GAPDH and normalized to the protein density measured at time 0. As seen, $Ca_V\beta3$ alone was more effective than $Ca_V\alpha2\delta1$ in preventing the degradation of $Ca_V1.2$, but co-expressing $Ca_V\beta3$ with $Ca_V\alpha2\delta1$ further stabilized the protein density of $Ca_V1.2$. The time courses of the protein degradation for the following conditions, $Ca_V1.2$ alone and $Ca_V1.2$/$Ca_V\alpha2\delta1$, were indistinguishable from one another and from the ΔMFI for FITC in the previous figure suggested that $Ca_V1.2$ (total density) was more stable in the presence of $Ca_V\alpha2\delta1$. This difference might arise from the higher sensitivity of the fluorescence assays. Molecular mass of $Ca_V1.2$ is ~250 kDa; $Ca_V\alpha2\delta1$ is 175 kDa; $Ca_V\beta3$ is 60 kDa; and GAPDH is 40 kDa. *E,* protein density was estimated with ImageJ (rsbweb.nih.gov). The time course of degradation was measured in three series of experiments. Each *symbol* represents the mean ± S.E. of the normalized protein density of $Ca_V1.2$.

tagged, confirmed the specificity of the FITC antibody in these series of experiments (data not shown). Given that the HA epitope is located in the extracellular portion of the protein, the fluorescence intensity for FITC obtained in the presence of intact cells reflects the cell surface density of $Ca_V1.2$. Fluorescence for FITC was measured after cell permeabilization to confirm the accessibility of the HA epitope. The fluorescence histograms are reported in Fig. 2, *A* and *B,* and the averaged mean fluorescence intensities are shown in Fig. 2*D*. $Ca_V\alpha2\delta$ alone improved total protein expression of $Ca_V1.2$ without any significant change in the cell surface density of $Ca_V1.2$. This contrasts with the impact of Cavβ (Fig. 2*D*) that improves both cell surface and total protein density of $Ca_V1.2$ (20). In particular, $Ca_V\beta3$ increased by ≈200% the cell surface density of $Ca_V1.2$, whereas $Ca_V\alpha2\delta$ barely stimulated cell surface density by 2 ± 3% (n = 3). Co-expression with both $Ca_V\beta3$ and $Ca_V\alpha2\delta$ did not increase cell surface detection of $Ca_V1.2$, although total protein stability was improved (Fig. 2, *A–D*). The former results contrast with confocal imaging data showing that co-expression with both $Ca_V\alpha2\delta$ and $Ca_V\beta1b$ is required to achieve the maximal cell surface staining for $Ca_V2.2$ (39). We had previously reported similar results with an HA-tagged $Ca_V1.2$ construct bearing its HA epitope in domain I (19).

The flow cytometry data were validated by cycloheximide chase analysis (Fig. 3, *A–C*). $Ca_V\beta3$ increased the protein expression of $Ca_V1.2$ in total lysates, whereas $Ca_V\alpha2\delta$ alone did not significantly alter protein density of $Ca_V1.2$. As seen in flow cytometry assays (Fig. 2*D*), total protein expression of $Ca_V1.2$ was also increased in the combined presence of $Ca_V\beta3$ and $Ca_V\alpha2\delta$ auxiliary subunits (Fig. 3, *D* and *E*), as also reported by others (20).

$Ca_V1.2$/$Ca_V\beta3$ Stabilizes the Expression of $Ca_V\alpha2\delta$—$Ca_V\beta$ subunits promote the cell surface density of $Ca_V1.2$, but little is known about their role on the trafficking of $Ca_V\alpha2\delta$. To investigate the trafficking of $Ca_V\alpha2\delta$, the pmCherry-$Ca_V\alpha2\delta$-HA

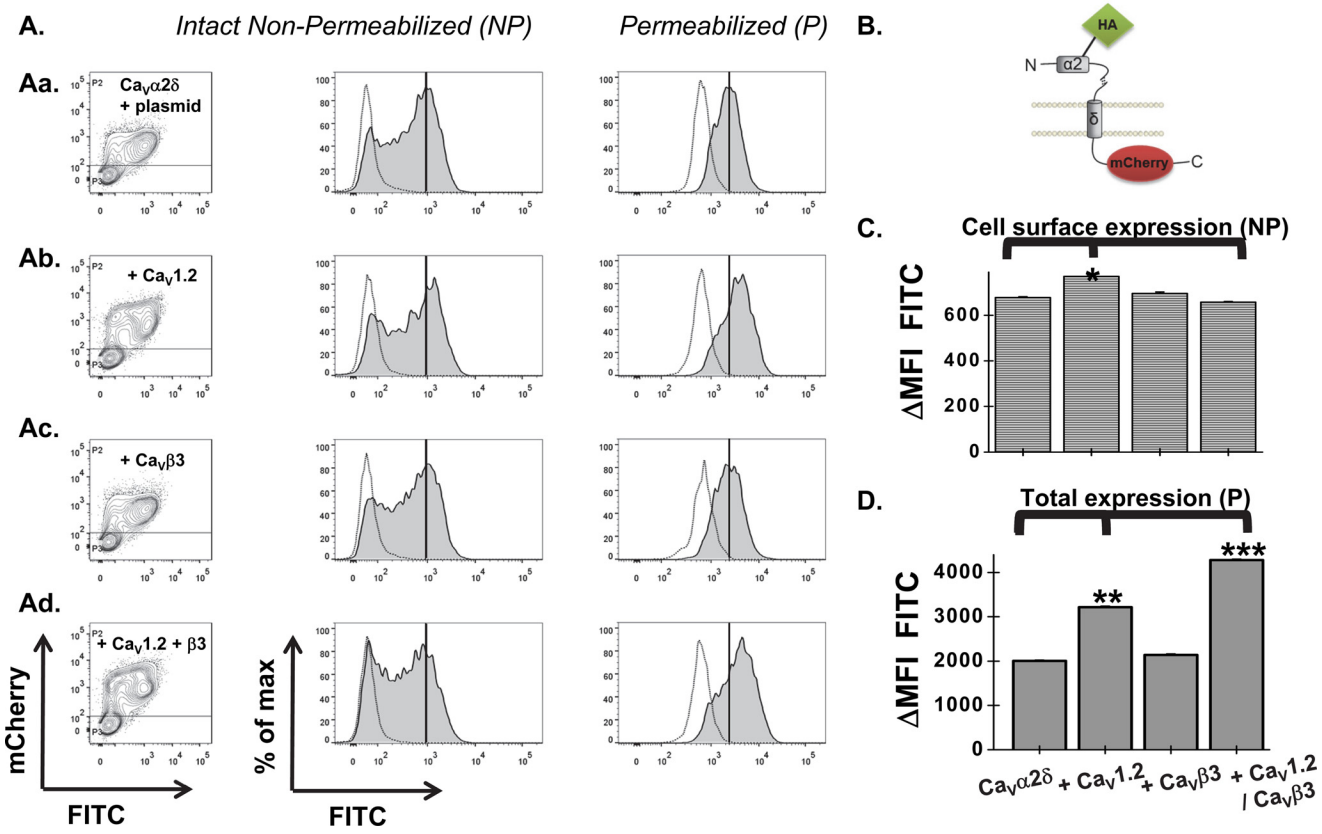

FIGURE 4. **Protein expression of $Ca_V\alpha2\delta1$ is increased in the presence of $Ca_V1.2$ and $Ca_V\beta3$.** *Aa,* pmCherry-$Ca_V\alpha2\delta1$-HA was transiently transfected with a control pCMV plasmid in HEKT cells; *Ab,* with $Ca_V1.2$ (untagged) in HEKT cells; *Ac,* in stable $Ca_V\beta3$ cells; and *Ad* with $Ca_V1.2$ (untagged) in stable $Ca_V\beta3$ cells. The HA tag of $Ca_V\alpha2\delta1$-HA was detected using an anti-HA FITC-conjugated antibody. Dead cells were excluded based on the forward scatter/side scatter profiles. Representative two-dimensional plots of mCherry *versus* FITC fluorescence are shown for each condition as stated (*left panels*). The *vertical line* indicates the median fluorescence intensity for FITC to facilitate the visual comparison between the different experimental groups. As seen, the cellular autofluorescence levels increased after permeabilization, which prevents comparison of the absolute fluorescence values between intact nonpermeabilized and permeabilized cells. *B,* predicted secondary structure of the pmCherry-$Ca_V\alpha2\delta1$-HA construct used in the figure. Please note that $Ca_V1.2$ was not tagged either in the N or C termini. *C, bar graph* shows the ΔMFI measured in the presence of FITC in intact cells for each experimental condition. Experiments were conducted in triplicate, and each *bar* is the mean ± S.E. of ΔMFI in arbitrary units. Under these conditions, ΔMFI measured for FITC reflects the relative cell surface protein expression of $Ca_V\alpha2\delta1$. *NP,* nonpermeabilized; *P,* permeabilized cells, *D, bar graph* shows the ΔMFI measured for FITC in permeabilized cells for each experimental condition. Experiments were conducted in triplicate, and each *bar* is the mean ± S.E. of ΔMFI in arbitrary units. Under these conditions, ΔMFI measured for FITC reflects the total protein expression of $Ca_V\alpha2\delta1$. *, $p < 0.05$; **, $p < 0.01$; ***, $p < 0.001$.

construct was expressed alone in HEKT and in stable $Ca_V\beta3$ cells in the presence or absence of $Ca_V1.2$. Two-color flow cytometry experiments were carried out in intact and permeabilized cells to respectively assess cell surface expression and total protein expression, the latter including cell surface and intracellular proteins. In two-dimensional plots, the fluorescence intensity obtained for mCherry was plotted against the fluorescence intensity for FITC. As seen in intact nonpermeabilized cells, the fluorescence intensity was strong for both mCherry and FITC indicating that $Ca_V\alpha2\delta$ is clearly present at the cell membrane (Fig. 4, *A* and *C*). Co-expression with $Ca_V\beta3$ alone did not significantly alter either surface or total expression, whereas co-expression with $Ca_V1.2$ only slightly improved cell surface and total protein expression of $Ca_V\alpha2\delta$. However, co-expression with both $Ca_V1.2$ and $Ca_V\beta3$ nearly doubled the total protein expression of $Ca_V\alpha2\delta$ but not its cell surface density. It is unlikely that the latter result was due to an unfavorable change in the conformation of the $Ca_V\alpha2\delta$-HA construct because $Ca_V1.2$ whole-cell currents were clearly up-regulated by $Ca_V\alpha2\delta$-HA in patch clamp experiments (see Fig. 1). The relative increase in total protein expression of $Ca_V\alpha2\delta$ was similar whether it was inferred from the constitutive mCherry fluorescence of mCherry-$Ca_V\alpha2\delta$-HA (data not shown) or from the FITC fluorescence in permeabilized cells (Fig. 4*D*). These results suggest that $Ca_V\alpha2\delta$ interacts intracellularly with $Ca_V1.2$ and that the stability of the protein complex is improved by $Ca_V\beta3$, probably in part driven by the nanomolar interaction between $Ca_V1.2$ and $Ca_V\beta3$ (41). Nonetheless, because the increase in total protein density did not translate into a surge in the cell surface density of $Ca_V\alpha2\delta$, it also suggests that most of the $Ca_V1.2$ protein complex remains in intracellular compartments.

Channel Modulation Depends upon the Cell Surface Expression of $Ca_V\alpha2\delta$—The correlation between the protein expression of $Ca_V\alpha2\delta$ and the modulation of $Ca_V1.2$ channels was quantified by co-expressing different DNA ratios of $Ca_V\alpha2\delta$ and $Ca_V1.2$. The ΔMFI values for FITC measured in intact and permeabilized cells increased steeply in the range from 1:20 to a 1:2 DNA ratio. Both the cell surface and the total protein densities followed a similar pattern (Fig. 5). Under our experimental conditions, the 1:1 DNA ratio yielded an additional 20% increase in the protein density, but raising further the relative amount of DNA coding for $Ca_V\alpha2\delta$ was found to impair trans-

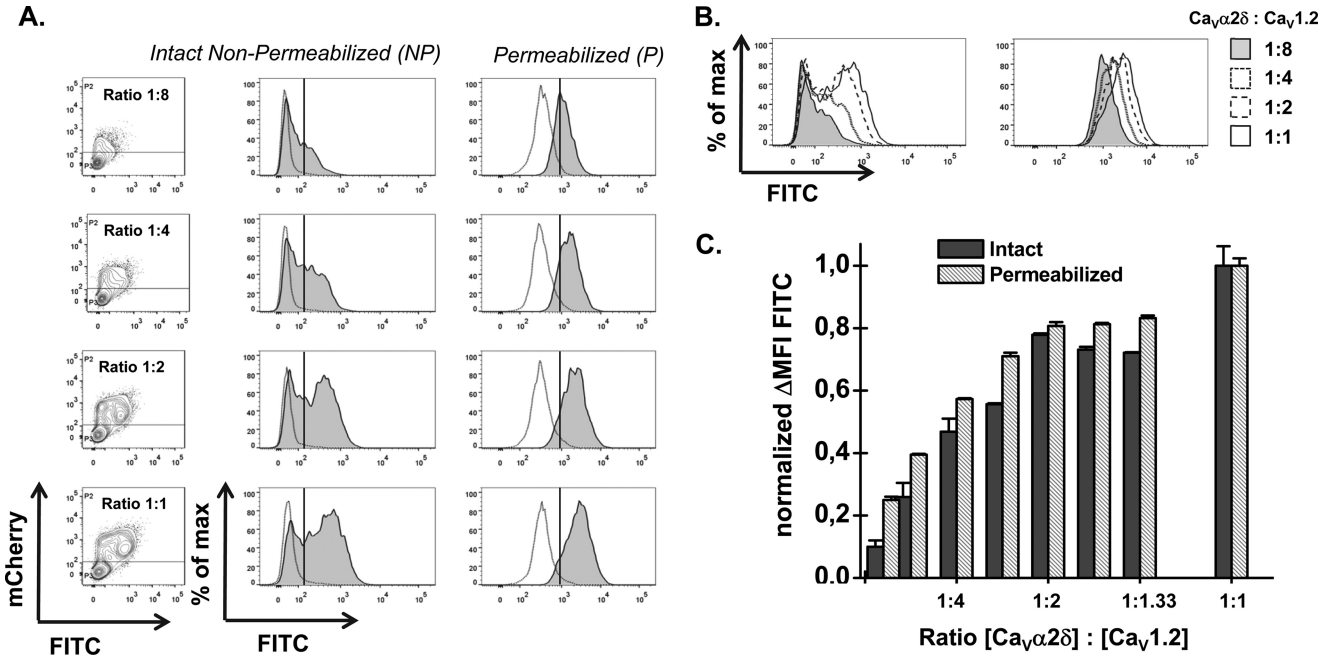

FIGURE 5. **Cell surface expression of $Ca_V\alpha2\delta1$ as a function of DNA ratios.** *A,* pmCherry-$Ca_V\alpha2\delta1$-HA WT (in variable amounts) was transiently transfected with $Ca_V1.2$ in stable $Ca_V\beta3$ cells. Protein expression was assessed in flow cytometry assays using the gating strategy explained in Fig. 4. Representative two-dimensional plots of mCherry *versus* FITC fluorescence are shown for each $Ca_V\alpha2\delta1$-HA/$Ca_V1.2$ DNA ratio as follows: ratio 1:8 (0.5 μg for $Ca_V\alpha2\delta1$-HA); ratio 1:4 (1 μg); ratio 1:2 (2 μg); and ratio 1:1 (4 μg) (*left panels*). Histogram plots show the distribution of fluorescence intensity of the anti-HA FITC-conjugated antibody staining in intact nonpermeabilized (*NP*) cells (*middle panels*) or in permeabilized (*P*) cells (*right panels*). *B,* overlay representation of the data is shown to facilitate visualization of the differences in fluorescence intensity as follows: Ratio 1:8 (*filled line*); ratio 1:4 (*dotted line*); ratio 1:2 (*dashed line*); and ratio 1:1 (*full line*). *C, bar graph* shows the normalized ΔMFI measured in the presence of FITC in intact nonpermeabilized (*dark gray bars*) and permeabilized (*hatched bars*) cells for $Ca_V\alpha2\delta1$-HA expressed in the combined presence of $Ca_V1.2$ and $Ca_V\beta3$. All ΔMFI values were normalized using the ΔMFI measured in the presence of a $Ca_V\alpha2\delta1$-HA/$Ca_V1.2$ DNA ratio of 1:1. As seen, the cell surface and total protein expression of $Ca_V\alpha2\delta1$ both increase steeply up to 1.5 to 2 μg of cDNA coding for $Ca_V\alpha2\delta1$-HA WT (ratios 1:3 to 1:2).

fection efficiency (data not shown). Patch clamp experiments established that increasing the cell surface expression of $Ca_V\alpha2\delta$ improves peak current density and activation gating of $Ca_V1.2$ (Fig. 6). Peak current density increased as a function of the cell surface density of $Ca_V\alpha2\delta$ within the range of our experimental conditions (Fig. 7). This suggests that increasing the cell surface density of $Ca_V\alpha2\delta$ improves the macroscopic activation gating of $Ca_V1.2$ by promoting the channel activation at more negative potentials.

Cell Surface Density Is Impaired in $Ca_V\alpha2\delta$ Genetic Variants—To gain further insight into the molecular mechanism underlying channel modulation by $Ca_V\alpha2\delta$, we turned to mutations of $Ca_V\alpha2\delta$ associated with cardiac arrhythmias. Burashnikov *et al.* (29) discovered 23 rare missense variants in three genes encoding subunits forming the $Ca_V1.2$ L-type calcium channel in 205 patients diagnosed with "J-wave syndromes." Four genetic variants were identified in the *CACNA2D1* gene encoding $Ca_V\alpha2\delta1$. The mutation S709N was found in two unrelated patients. Two mutations (D550Y and Q917H) were identified in the same individual (29), but their expression profile has yet to been fully characterized (32). $Ca_V\alpha2\delta$ missense mutants D550Y, S709N, Q917H, S956T, the double D550Y/Q917H (29), as well as $Ca_V\alpha2\delta$ S755T mutant associated with SQTS6 (31) were expressed alone or in combination with $Ca_V1.2$ and $Ca_V\beta3$, the same subunit composition we used for functional characterization in patch clamp experiments. These six $Ca_V\alpha2\delta$ mutations were co-expressed with $Ca_V1.2$ WT (no HA) in the maximum 1:1 ratio in stable $Ca_V\beta3$ cells. The transfection efficiency (as assessed by the number of fluorescent cells) was found to be not significantly different between the HA-tagged $Ca_V\alpha2\delta$ WT and the HA-tagged $Ca_V\alpha2\delta$ mutant constructs. Overall, the total protein density of all mutants estimated from permeabilized cells or from the constitutive mCherry fluorescence (data not shown) significantly increased in the combined presence of $Ca_V1.2$ and $Ca_V\beta3$. As shown in Figs. 8 and 9, the ΔMFI for FITC of $Ca_V\alpha2\delta$ S755T, Q917H, and S956T mutants in intact cells under these conditions was similar to the ΔMFI measured for $Ca_V\alpha2\delta$-HA WT suggesting that the cell surface density of $Ca_V\alpha2\delta$ was not affected by these single mutations. In contrast, missense mutations D550Y and S709N and more significantly the double mutant D550Y/Q917H impaired the cell surface targeting of $Ca_V\alpha2\delta$-HA with ≈30% reduction for the former mutants and ≈60% decrease for the latter. Doubling the amount of cDNA used for transfection did not improve cell surface expression because the transfection efficiency decreased with larger DNA concentrations. The surface density of D550Y/Q917H proteins remained on average 60% lower than the one measured for the $Ca_V\alpha2\delta$-HA WT protein at each DNA ratio tested from 1:20 (data not shown) to 1:1. Flow cytometry assays carried out 36 h after transfection yielded similar results suggesting that a 24-h culture time is sufficient to observe the optimal protein expression (data not shown). The fluorescence intensities for FITC in permeabilized cells and for the constitutive mCherry were only decreased by ≈30% when compared with the signals measured for

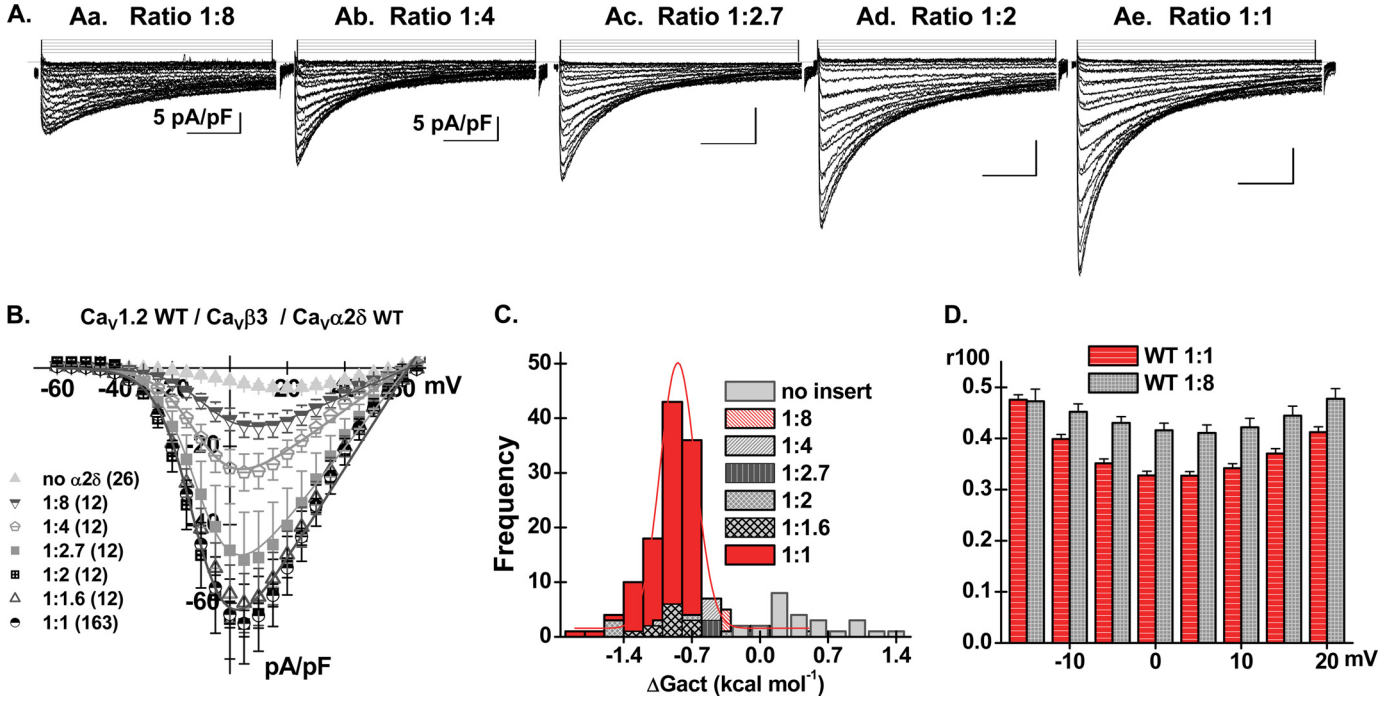

FIGURE 6. **Modulation of L-type $Ca_V1.2$ currents parallels the cell surface expression of $Ca_V\alpha2\delta1$.** *A,* pCMV-$Ca_V1.2$ (untagged) was co-expressed in stable $Ca_V\beta3$ cells with variable pmCherry-$Ca_V\alpha2\delta1$-HA DNA ratios for $Ca_V\alpha2\delta/Ca_V1.2$ as follows: *Aa,* ratio 1:8 (0.5 μg); *Ab,* ratio 1:4 (1 μg); *Ac,* ratio 1:2.7 (1.5 μg); *Ad,* ratio 1:2 (2 μg); and *Ae,* ratio 1:1 (4 μg). Typical whole-cell current traces were recorded in a 2 mM Ca^{2+} solution from a holding potential of −100 mV. The pmCherry-$Ca_V\alpha2\delta1$-HA construct used for the patch clamp experiments was identical to the constructs studied in the flow cytometry assays. Time scale is 100 ms throughout. Unless specified otherwise, the current density scale is 10 pA/pF. *B,* peak current densities increased from −5 ± 1 pA/pF (n = 26) (no insert in the pmCherry vector) to −67 ± 3 pA/pF (n = 163) in the presence of 4 μg of cDNA (ratio 1:1) coding for pmCherry-$Ca_V\alpha2\delta1$-HA WT. The number in *parentheses* indicates the number of independent patch clamp recordings. *C,* histogram reporting the distribution of the individual ΔG_{act} values (kilocalories/mol) for each concentration of cDNA coding for $Ca_V\alpha2\delta1$. As seen, the ΔG_{act} are significantly shifted to the left even when $Ca_V1.2$ is co-expressed with $Ca_V\alpha2\delta1$ in a 1:1 ratio. *D,* inactivation kinetics of the $Ca_V1.2$ currents expressed with $Ca_V\alpha2\delta1$ in a 1:8 ratio (*gray hatched bars*) were in general 20% slower ($p < 0.05$) than the inactivation kinetics measured after co-expression of $Ca_V\alpha2\delta1$ in a 1:1 ratio (*white striated red bars*) ($p < 0.05$).

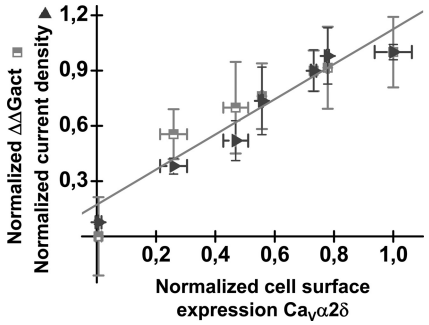

FIGURE 7. **Correlation between the cell surface density of $Ca_V\alpha2\delta1$-HA WT and the changes in ΔG_{act} and peak current density of $Ca_V1.2$ currents.** Peak current density was normalized to the mean value measured with 4 μg of cDNA for $Ca_V\alpha2\delta1$-HA (ratio 1:1); $\Delta\Delta G_{act}$ was calculated relative to the value of ΔG_{act} = 0.48 ± 0.09 kcal mol^{-1} for currents measured in the absence of $Ca_V\alpha2\delta1$; the cell surface density was computed using the normalized ΔMFI measured for FITC in intact nonpermeabilized cells. Despite the large experimental variation, there is a positive correlation between the cell surface density of $Ca_V\alpha2\delta1$ and the two other parameters (peak current density and $\Delta\Delta G_{act}$ of macroscopic currents). The variation of $\Delta\Delta G_{act}$ with the surface density of $Ca_V\alpha2\delta1$ suggests that $Ca_V\alpha2\delta1$ influences the fraction of ion channels active in a given gating mode. The correlation could be described by a large number of equations, but it is shown as a linear regression to facilitate visualization.

$Ca_V\alpha2\delta$-HA WT. These data indicate the following: (*a*) HA tag remained accessible in the double mutant; (*b*) the cell and the total protein density were both affected by the D550Y/Q917H double mutation albeit to a different extent. Altogether, these data suggest that the double mutation impairs the trafficking of $Ca_V\alpha2\delta$ to a greater extent than protein stability.

Channel Modulation Is Altered in the Presence of $Ca_V\alpha2\delta$ Genetic Variants—The functional impact of the missense $Ca_V\alpha2\delta$ mutations was characterized by electrophysiology after co-expression of $Ca_V1.2$ and $Ca_V\alpha2\delta$ in stable $Ca_V\beta3$ cells. In the presence of a 1:1 ratio, the five single point mutations, including D550Y and S709N, increased $Ca_V1.2$ peak current densities by 10–13-fold with a negative shift in the voltage-dependent gating activation ($\Delta G_{act} \approx -1$ kcal mol^{-1}) in a fashion reminiscent of $Ca_V\alpha2\delta$ WT (Table 1). Hence, $Ca_V\alpha2\delta$ D550Y and S709N mutations boosted the peak current densities despite a 30% decrease in the cell surface expression of $Ca_V\alpha2\delta$. These results are in agreement with Fig. 7 showing that an ≈30% decrease in the cell surface density of $Ca_V\alpha2\delta$ is not sufficient to significantly prevent the up-regulation of macroscopic $Ca_V1.2$ currents. In contrast, co-expression of $Ca_V\alpha2\delta$-HA D550Y/Q917H produced currents that were 35% lower than $Ca_V\alpha2\delta$-HA WT with an average of −40 ± 10 pA/pF (n = 10) compared with −67 ± 3 pA/pF (n = 163) (Fig 10). The experimental variation, however, limits the statistical significance to $p < 0.5$. Nonetheless, there seems to be a trend toward a decreased function that was also reported by the authors of the original paper (29). We hypothesized that the decrease in the cell surface density of the $Ca_V\alpha2\delta$ D550Y/Q917H mutant could become more significant when expressing $Ca_V\alpha2\delta/Ca_V1.2$ in a 1:20 ratio. Patch clamp experiments

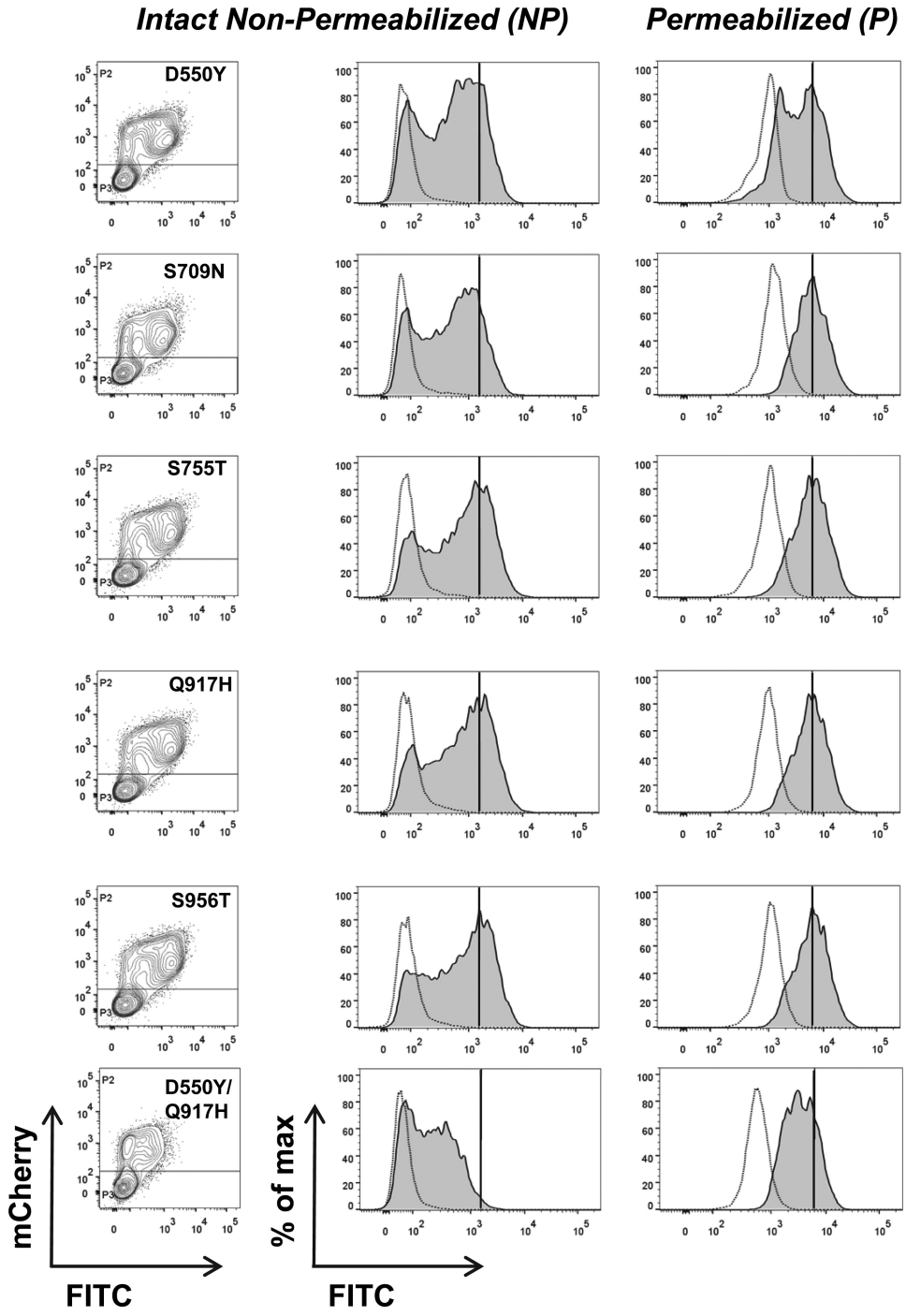

FIGURE 8. **Cell surface and total protein expression of $Ca_V\alpha2\delta1$ D550Y/Q917H mutant is significantly decreased.** pmCherry-$Ca_V\alpha2\delta1$-HA WT and mutants were transiently transfected with pCMV-$Ca_V1.2$ (untagged) in stable $Ca_V\beta3$ cells. Fluorescence was computed according to the gating strategy described under "Experimental Procedures" and in Fig. 4. Representative two-dimensional plots of mCherry *versus* FITC fluorescence (*left panels*) are shown for each $Ca_V\alpha2\delta1$ mutant as follows: D550Y, S709N, S755T, Q917H, S956T, and D550Y/Q917H (from *top to bottom*). Histogram plots show the distribution of fluorescence intensity for the anti-HA FITC conjugated antibody staining in intact nonpermeabilized (*NP*) cells (*middle panels*) or in permeabilized (*P*) cells (*right panels*). The median fluorescence intensity of FITC is indicated by a straight line on the histograms to help comparison between the different mutants. Increasing the DNA amount to 8 μg ($Ca_V\alpha2\delta/Ca_V1.2$ DNA ratio of 2:1) did not increase further the surface expression of D550Y/Q917H.

were thus carried out with cDNA ratios of 1:1, 1:8, and 1:20 $Ca_V\alpha2\delta/Ca_V1.2$ (0.2:4 μg of DNA) (Fig 11). As shown, the behavior of the double mutant departed more significantly from the wild-type protein at lower cDNA concentrations. It is interesting to note that the decrease in peak current density was accompanied by a rightward shift in the activation potentials. Altogether, our results suggest that some $Ca_V\alpha2\delta$ arrhythmogenic mutations may decrease $Ca_V1.2$ currents in cardiomyocytes as a result of their decreased cell surface density.

DISCUSSION

$Ca_V\alpha2\delta$ Improves the Stability of $Ca_V1.2$-$Ca_V\beta$ Complexes—It is generally agreed that recombinant expression of $Ca_V\alpha2\delta$ boosts peak current density of $Ca_V1.2$ in recombinant cells (19)

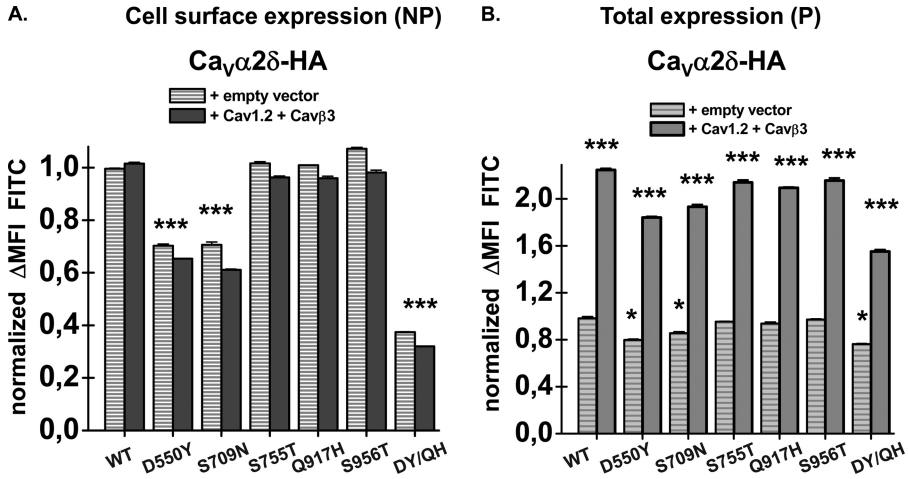

FIGURE 9. *A, bar graph* shows the normalized ΔMFI measured in the presence of FITC in intact cells for each pmCherry-$Ca_V\alpha2\delta1$-HA construct (WT and mutants) expressed alone (*hatched bars*) and in the presence of $Ca_V1.2$ (untagged) in stable $Ca_V\beta3$ cells (*dark gray bars*). As seen, the relative cell surface density measured in intact cells decreased by 29 ± 2, 31 ± 3, and 63 ± 1% for $Ca_V\alpha2\delta1$ mutants D550Y, S709N, and the double mutant D550Y/Q917H (shown as *DY/QH*), respectively, when expressed alone (*hatched bars*) or in stable $Ca_V\beta3$ cells with $Ca_V1.2$ (*filled dark gray bars*). Values were normalized as compared with the ΔMFI for FITC measured for $Ca_V\alpha2\delta1$-HA WT under the same experimental conditions ($p < 0.001$). *NP*, nonpermeabilized. *B, bar graph* shows the ΔMFI measured for FITC in permeabilized (*P*) cells for each $Ca_V\alpha2\delta1$-HA construct (WT and mutants) expressed alone (*hatched bars*) or in stable $Ca_V\beta3$ cells with $Ca_V1.2$ (*filled gray bars*). All ΔMFI values were normalized as compared with the average ΔMFI measured with $Ca_V\alpha2\delta1$-HA WT expressed alone in HEKT cells. ΔMFI for FITC measured in permeabilized cells reflects the total protein expression of $Ca_V\alpha2\delta1$-HA constructs. As seen, the total protein density decreased by 20 ± 1, 21 ± 2, and 24 ± 11% for $Ca_V\alpha2\delta1$-HA D550Y, S709N, and D550Y/Q917H, respectively ($p < 0.05$), when compared with the wild-type construct. This small decrease in total protein density of these mutants could account in part for their decreased cell surface density. This decrease was also observed for the constitutive fluorescence of mCherry (data not shown). For all mutants, please note that the total protein density of all $Ca_V\alpha2\delta1$-HA constructs nearly doubled when co-expressed with $Ca_V1.2$ in stable $Ca_V\beta3$ cells. *, $p < 0.05$; ***, $p < 0.001$.

TABLE 1

Biophysical properties of $Ca_V1.2$/ $Ca_V\beta3$ channels with and without $Ca_V\alpha2\delta1$

$Ca_V1.2$ WT was expressed in stable $Ca_V\beta3$ cells with pmCherry-no insert or pmCherry-$Ca_V\alpha2\delta$ construct under typical conditions with a 1:1 DNA ratio (4 μg: 4 μg). Biophysical parameters were measured in the presence of 2 mM Ca^{2+} as described elsewhere (19). Activation properties ($E_{0.5,\,act}$ and ΔG_{act}) were estimated from the mean *I-V* relationships and fitted to a Boltzmann equation. The data are shown with the mean ± S.E. of the individual experiments, and the number of experiments is in parentheses. ND means not determined as the signal-to-noise ratio was too small in the absence of $Ca_V\alpha2\delta1$.

$Ca_V1.2$ WT in $Ca_V\beta3$ stable HEKT cells with 2 mM Ca^{2+}	Electrophysiological properties			
	$E_{0.5,\,act}$	ΔG_{act}	Peak density	r100 at +5 mV
	mV	*kcal mol*$^{-1}$	*pA/pF*	
No $Ca_V\alpha2\delta1$-HA (pmCherry-no insert)	4 ± 1 (26)	0.5 ± 0.1 (26)	−5.4 ± 0.7 (26)	ND
+ $Ca_V\alpha2\delta1$ WT no HA (1:1 ratio)	−10.1 ± 0.5 (23)	−0.86 ± 0.05 (23)	−56 ± 3 (23)	0.31 ± 0.02 (23)
+ $Ca_V\alpha2\delta1$-HA WT (1:1 ratio)	−10.6 ± 0.2 (163)	−0.90 ± 0.03 (163)	−67 ± 3 (163)	0.38 ± 0.02 (163)
+ $Ca_V\alpha2\delta1$-HA D550Y (1:1 ratio)	−10.9 ± 0.7 (10)	−0.9 ± 0.1 (10)	−61 ± 9 (10)	0.33 ± 0.01 (10)
+ $Ca_V\alpha2\delta1$-HA S709N (1:1 ratio)	−11.3 ± 0.6 (10)	−0.9 ± 0.1 (10)	−49 ± 10 (10)	0.37 ± 0.02 (10)
+ $Ca_V\alpha2\delta1$-HA S755T (1:1 ratio)	−11.4 ± 0.4 (20)	−1.0 ± 0.0 (20)	−73 ± 10 (20)	0.29 ± 0.02 (20)
+ $Ca_V\alpha2\delta1$-HA Q917H (1:1 ratio)	−11.4 ± 0.7 (10)	−1.0 ± 0.1 (10)	−69 ± 9 (10)	0.37 ± 0.02 (10)
+ $Ca_V\alpha2\delta1$-HA S956T (1:1 ratio)	−10.8 ± 0.6 (10)	−0.9 ± 0.1 (10)	−84 ± 9 (10)	0.33 ± 0.02 (10)
+ $Ca_V\alpha2\delta1$-HA D550Y/ Q917H (1:1 ratio)	−9 ± 2 (10)	−0.8 ± 0.2 (10)	−40 ± 10 (10)	0.35 ± 0.03 (10)

as well as in native mouse cardiomyocytes (21). Whether this modulation is conveyed through an increase in the cell surface density of $Ca_V1.2$ remains debated (19, 20, 42) in part because the macroscopic peak current density is the product of three parameters as follows: the number of channels in the plasma membrane, the open channel probability, and the single-channel conductance. We have opted to investigate changes in the channel surface density using a sensitive and high throughput flow cytometry fluorescence-based assay. In this assay, the cell samples go through a gating process that excludes dead cells, debris, and aggregates such that the fluorescence intensity reflects protein expression in intact cells of similar morphological properties. This approach required the insertion of a 9-residue HA epitope in the extracellular face of the $Ca_V1.2$ pore-forming subunit. Such manipulation may interfere with protein expression and/or interaction with other subunits as shown very elegantly in Ref. 39. Indeed, we have tested many constructs before identifying one that preserves the up-regulation of $Ca_V1.2$ currents by $Ca_V\alpha2\delta$. As shown in the first series of experiments, whole-cell currents measured with the HA-tagged version of $Ca_V1.2$ were functionally up-regulated by the tagged and the untagged versions of $Ca_V\alpha2\delta$. Using the untagged version of $Ca_V\alpha2\delta$, we evaluated the changes in the surface and the total protein expression of HA-$Ca_V1.2$ from the relative fluorescence of the FITC-conjugated antibody in intact and permeabilized cells. Total protein density was also measured using Western blotting. Altogether, our results show the following: (*a*) $Ca_V\alpha2\delta$ alone, unlike $Ca_V\beta$ (20, 35), does not prevent the degradation or improve the cell surface density of $Ca_V1.2$ proteins; and (*b*) in the presence of $Ca_V\beta3$, $Ca_V\alpha2\delta$ improves the stability and/or the total protein expression of $Ca_V1.2$ proteins. Hence, we show that $Ca_V\alpha2\delta$ up-regulates $Ca_V1.2$ currents by improving the channel activation gating without significantly increasing the number of $Ca_V1.2$ proteins at the cell surface.

Recombinant $Ca_V\alpha2\delta$ Is Strongly Expressed at the Membrane—The trafficking of $Ca_V\alpha2\delta$ was studied using a similar fluorescence-based assay, but surface and total protein density were

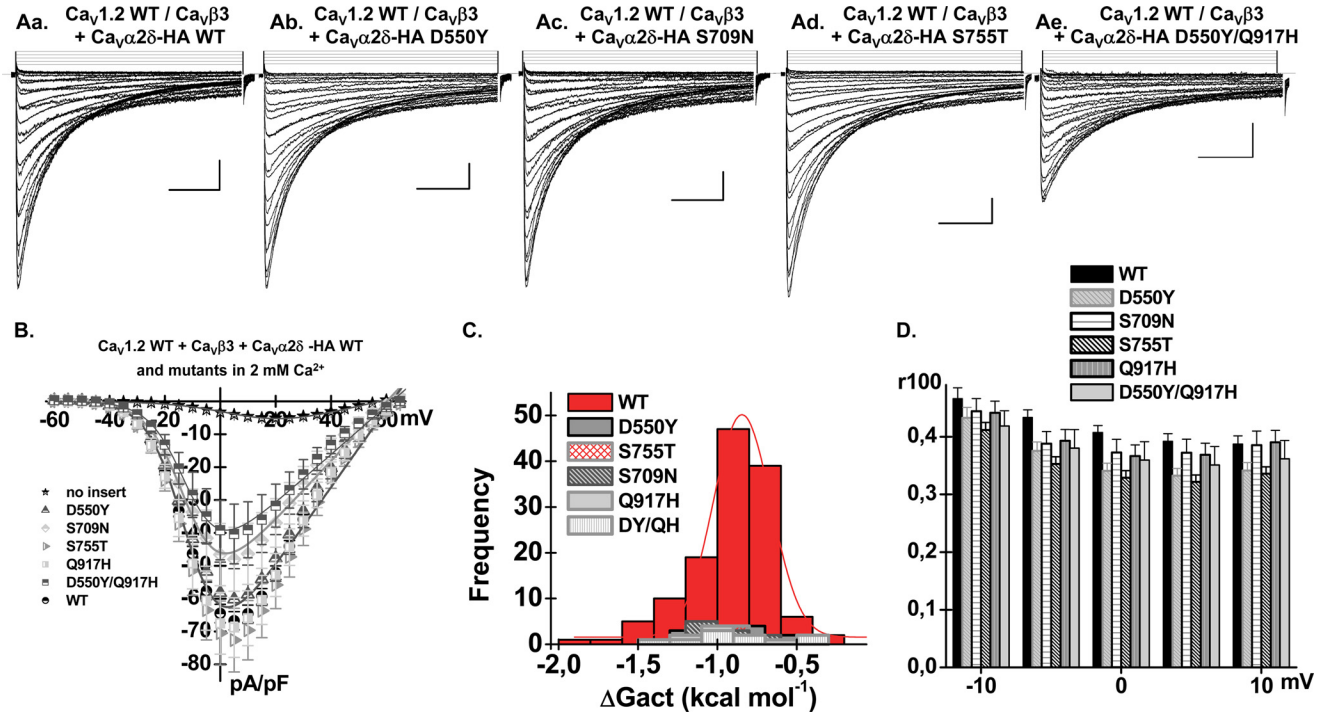

FIGURE 10. **$Ca_V\alpha2\delta1$ short QT mutants functionally modulate the L-type $Ca_V1.2$ currents.** *A,* pCMV-$Ca_V1.2$ was co-expressed in stable $Ca_V\beta3$ stable cells with the following: $Ca_V\alpha2\delta1$WT (*Aa*); $Ca_V\alpha2\delta1$ D550Y (*Ab*); (*Ac*) $Ca_V\alpha2\delta1$ S709N; $Ca_V\alpha2\delta1$ S755T (*Ad*); and $Ca_V\alpha2\delta1$ D550Y/Q917H (*Ae*). Typical whole-cell current traces were recorded in a 2 mM Ca^{2+} solution from a holding potential of −100 mV. The pmCherry-$Ca_V\alpha2\delta1$-HA constructs were identical to the constructs used for the flow cytometry assays. Time scale is 100 ms throughout. Unless specified otherwise, the current density scale is 10 pA/pF. *B,* peak current densities increased from −5 ± 1 pA/pF ($n = 26$) (no insert in the pmCherry vector) to −67 ± 3 pA/pF ($n = 163$) in the presence of pmCherry-$Ca_V\alpha2\delta1$-HA WT ($p < 10^{-6}$). Co-expression with $Ca_V\alpha2\delta$ D550Y/Q917H significantly increased peak current densities of $Ca_V1.2$ as compared with the currents obtained in the absence of $Ca_V\alpha2\delta$ and did not produce currents significantly different from $Ca_V\alpha2\delta1$ WT ($p > 0.1$) with a value of 40 ± 10 pA/pF ($n = 10$). The properties of $Ca_V\alpha2\delta1$ mutants were estimated from 10 to 15 independent patch clamp recordings. *C,* histogram reporting the distribution of the individual ΔG_{act} values (kilocalories/mol) for each $Ca_V\alpha2\delta1$ mutant. As seen, every single $Ca_V\alpha2\delta$ mutant negatively shifted the activation energy of $Ca_V1.2$ with a distribution of ΔG_{act} values that superimposed with the ΔG_{act} values of the $Ca_V\alpha2\delta1$ WT. *D, bar graph* shows the r100 values (the ratio of peak whole-cell currents remaining at the end of a 100-ms depolarization) measured at membrane potentials from −10 to +10 mV. Faster inactivation kinetics yield lower r100 values. Inactivation kinetics of the $Ca_V1.2$ currents expressed with the $Ca_V\alpha2\delta1$ mutants S709N and Q917H were not significantly different from the ones measured in the presence of $Ca_V\alpha2\delta1$ WT. The r100 values of $Ca_V\alpha2\delta1$ mutants D550Y and S755T were 15% smaller suggesting faster inactivation kinetics for these $Ca_V\alpha2\delta1$ mutants. *, $p < 0.05$.

tracked by the external HA epitope and the intracellular mCherry tag, respectively. The constitutive mCherry fluorescence was used as an index of $Ca_V\alpha2\delta$ expression under all conditions for the wild-type protein as well as the $Ca_V\alpha2\delta$ mutants (see below). Patch clamp experiments carried out with the untagged version of $Ca_V1.2$ but using the HA-tagged mCherry $Ca_V\alpha2\delta$ constructs (WT and mutants) confirmed the latter construct was functional. It is essential to stress that fluorescence cell sorting experiments (protein expression) and whole-cell recordings (channel function) were carried out with cells grown under the same conditions. These data validated that the double modification, insertion of the HA epitope and the mCherry protein, did not prevent functional modulation of the L-type currents by $Ca_V\alpha2\delta$. Furthermore, the accessibility of the HA epitope was validated in each flow cytometry assay by comparing the relative fluorescence intensities obtained with the FITC-conjugated antibody in permeabilized cells with the constitutive mCherry in intact and permeabilized cells.

$Ca_V\alpha2\delta$ was shown to reach the cell surface when expressed alone (our data in HEKT cells and see Ref. 42). The strong fluorescence intensity suggests that the cell surface density of $Ca_V\alpha2\delta$ is larger than the cell surface density of $Ca_V1.2$ expressed under similar conditions. Similar observations were made in mouse cardiomyocytes showing that endogenous $Ca_V\alpha2\delta$ is significantly expressed at the plasma membrane (Fig 12). Co-expression with $Ca_V\beta3$ did not appreciably alter the cell surface density of $Ca_V\alpha2\delta$ in contrast to what we and others have reported for the $Ca_V\alpha1$ subunit of $Ca_V1.2$ (19). Nonetheless, our study highlighted some reciprocal modulation within the proteins forming the L-type $Ca_V1.2$ channel. Indeed, the total protein expression of $Ca_V\alpha2\delta$ significantly improved in the combined presence of $Ca_V1.2$ and $Ca_V\beta3$. The significant increase of total protein expression in the combined presence of $Ca_V1.2$ and $Ca_V\beta3$ measured from the relative fluorescence for FITC in permeabilized cells did not result from an improved accessibility of the HA epitope because the constitutive mCherry fluorescence as well as the total protein density measured in Western blots were similarly augmented. Furthermore, our results show that the modulation of L-type currents is a quasi-linear function of the cell surface density of $Ca_V\alpha2\delta$. It suggests that the interaction between $Ca_V1.2$ and $Ca_V\alpha2\delta$ is conveyed through one or multiple low affinity binding site(s).

Cardiac Arrhythmias and $Ca_V\alpha2\delta$—In the context where the numbers of channelopathy susceptibility genes and mutations identified are increasing rapidly, there is renewed interest in characterizing the molecular mechanisms underlying modulation of L-type $Ca_V1.2$ channels by its auxiliary subunits, in particular $Ca_V\alpha2\delta$. In return, structure-function insights gleaned

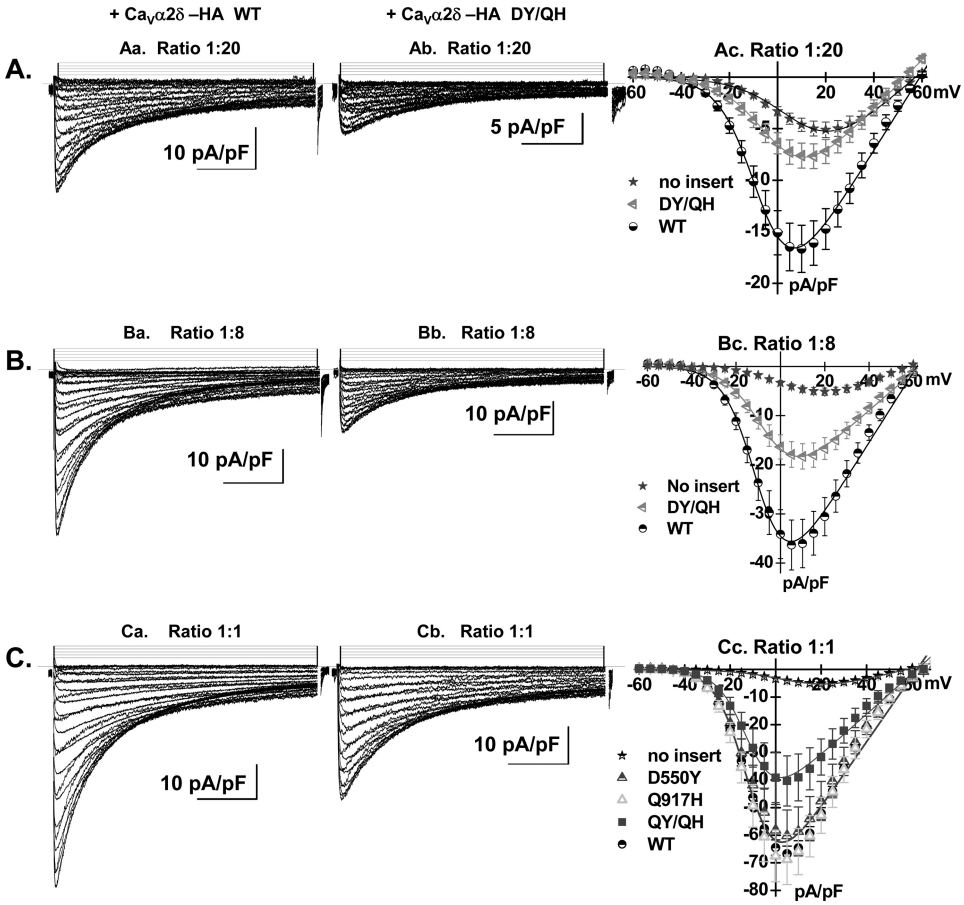

FIGURE 11. **L-type $Ca_V1.2$ currents are impaired in the presence of $Ca_V\alpha2\delta1$ D550Y/Q917H mutant.** pCMV-$Ca_V1.2$ (untagged) was co-expressed in stable $Ca_V\beta3$ stable cells with pmCherry-$Ca_V\alpha2\delta$-HA WT or pmCherry-$Ca_V\alpha2\delta$-HA D550Y/Q917H (*DY/QH*) at the cDNA ratios indicated for $Ca_V\alpha2\delta/Ca_V1.2$. Typical whole-cell current traces were recorded in a 2 mM Ca^{2+} solution from a holding potential of −100 mV. Time scale is 100 ms throughout. *A,* DNA ratio for $Ca_V\alpha2\delta/Ca_V1.2$ of 1:20 with 0.2 μg of DNA for $Ca_V\alpha2\delta$-HA. *Aa,* $Ca_V\alpha2\delta$-HA WT; *Ab,* $Ca_V\alpha2\delta$-HA D550Y/Q917H; *Ac,* average peak current densities increased from −5 ± 1 pA/pF ($n = 26$) (no insert in the pmCherry vector) to −7 ± 1 pA/pF ($n = 9$) for mCherry-$Ca_V\alpha2\delta1$-HA D550Y/Q917H, and −17 ± 2 pA/pF ($n = 4$) for WT ($p < 10^{-6}$). Co-expression with $Ca_V\alpha2\delta$ D550Y/Q917H significantly increased peak current densities of $Ca_V1.2$ as compared with the currents obtained in the absence of $Ca_V\alpha2\delta$ but were significantly different from $Ca_V\alpha2\delta1$ WT ($p < 0.05$). The ΔG_{act} (in kcal mol^{-1}) values were −0.02 ± 0.01 for D550Y/Q917H and −0.30 ± 0.05 for WT. *B,* DNA ratio for $Ca_V\alpha2\delta/Ca_V1.2$ of 1:8 with 0.5 μg of DNA for $Ca_V\alpha2\delta$-HA. *Ba,* $Ca_V\alpha2\delta$-HA WT; *Bb,* $Ca_V\alpha2\delta$-HA D550Y/Q917H; *Bc,* average peak current densities were −18 ± 3 pA/pF ($n = 12$) for mCherry-$Ca_V\alpha2\delta1$-HA D550Y/Q917H, and −36 ± 5 pA/pF ($n = 12$) for WT. Co-expression with $Ca_V\alpha2\delta$ D550Y/Q917H significantly increased peak current densities of $Ca_V1.2$ as compared with the currents obtained in the absence of $Ca_V\alpha2\delta$ but were significantly different from $Ca_V\alpha2\delta1$ WT ($p < 0.05$). The ΔG_{act} (in kilocalories mol^{-1}) values were −0.29 ± 0.03 for D550Y/Q917H and −0.57 ± 0.09 for WT. *C,* DNA ratio for $Ca_V\alpha2\delta/Ca_V1.2$ was 1:1 with 4 μg of DNA for $Ca_V\alpha2\delta$. *Ca,* $Ca_V\alpha2\delta1$WT; *Cb,* $Ca_V\alpha2\delta1$ D550Y/Q917H; *Cc,* average peak current densities are shown under these conditions. QY/QH should read DY/QH for D550Y/Q917H. Numerical values are shown in Table 1. Co-expression with $Ca_V\alpha2\delta$ D550Y/Q917H significantly increased peak current densities of $Ca_V1.2$ as compared with the currents obtained in the absence of $Ca_V\alpha2\delta$ and were significantly different from $Ca_V\alpha2\delta1$ WT ($p > 0.1$).

from these disease susceptibility genes have significantly advanced our understanding of the pathophysiology of these syndromes and have paved the way to the development of new treatment strategies. Over the last few years, single missense mutations and/or genetic variants of $Ca_V\alpha2\delta$ have been identified in patients experiencing cardiac arrhythmias associated with repolarizing QT interval (SQT) shorter than normal. Short QT arrhythmias are generally associated with gain-of-function outward currents (potassium currents) or loss-of-function of inward (sodium or calcium) currents. At the time of their identification, the missense mutations in $Ca_V\alpha2\delta$ have been labeled loss-of-function mutations and were proposed to alter L-type $Ca_V1.2$ peak current density through a change in the membrane expression of $Ca_V1.2$ (29). Having established a reliable experimental model to define the surface expression and the function of the different components of the L-type $Ca_V1.2$ channel, we explored the impact of $Ca_V\alpha2\delta$ mutations associated with sudden cardiac death. Recombinant expression in HEKT cells of $Ca_V\alpha2\delta$ single mutants S755T, Q917H, and S956T associated with shorter QT intervals did not cause any significant change in the cell surface expression of $Ca_V\alpha2\delta$ or in the function of $Ca_V1.2$ currents when expressed using a 1:1 cDNA ratio. This is true also for the mutation $Ca_V\alpha2\delta$ S755T that was reported by others to prevent the up-regulation of $Ca_V1.2$ currents by $Ca_V\alpha2\delta$ in HEKT cells (31). In contrast, we have observed a, ≈30% decrease in the cell surface density of $Ca_V\alpha2\delta$ D550Y and S709N single mutants accompanied with an ≈15% in the total protein density that remained unchanged up to 36 h after transfection. Despite causing a reduction in the cell surface expression of $Ca_V\alpha2\delta$, the single mutants D550Y and S709N did not significantly impair the modulation of $Ca_V1.2$ currents when co-expressed in a 1:1 cDNA ratio. Combining two mutations in $Ca_V\alpha2\delta$ with D550Y/Q917H significantly reduced the cell surface density of $Ca_V\alpha2\delta$ (60%) under the same conditions. Although both the cell surface and the total protein density of the double mutant were reduced, the decrease in the cell surface

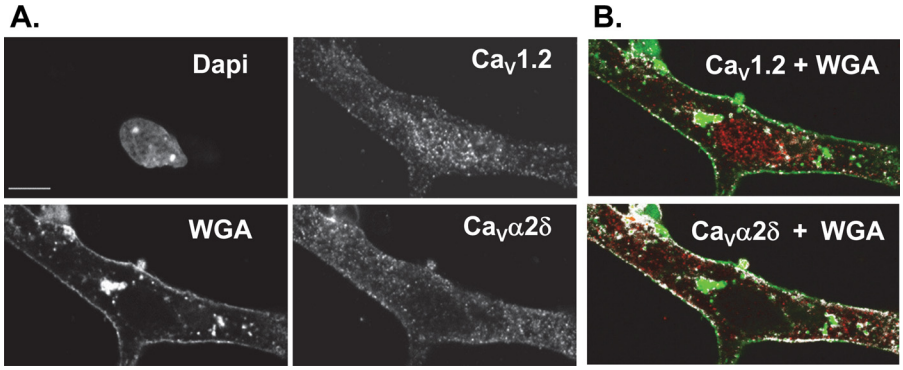

FIGURE 12. **Co-localization of endogenous $Ca_V1.2$ and $Ca_V\alpha2\delta$ at the plasma membrane in 24-h post-culture myocytes.** Ventricles of 1–3-day-old CD1 mice were digested with collagenase type II (Worthington). Cardiomyocytes were collected by centrifugation and cultured at 37 °C in a 5% CO_2 incubator for 24 h in M199 culture medium (Invitrogen) containing 15% fetal bovine serum. *A,* nuclei were stained with DAPI (1:1000) (Invitrogen). Cultured cells were incubated with wheat germ agglutinin (*WGA*) 647 (1:200) (Invitrogen) for 10 min and fixed in 2% paraformaldehyde at room temperature for 15 min followed by a final incubation with 0.1% Triton X-100 for 60 min. After overnight incubation at 4 °C with either primary anti-$Ca_V1.2$ (1:100) (Alomone Labs) and anti-$Ca_V\alpha2\delta$ (1:50) (Santa Cruz Biotechnology) antibodies in 1% donkey serum with 0.05% Triton X-100, cells were incubated with Alexa 555 for $Ca_V1.2$ (1:800) and Alexa 488 for $Ca_V\alpha2\delta$ (1:800) secondary antibodies (Invitrogen) for 90 min at room temperature. Confocal fluorescent images were captured with a Zeiss LSM 710 confocal microscope system with ×63/1.40 oil objective. *Scale bar* corresponds to 10 μm. The images were analyzed using FIJI software. *B, red channel* (either $Ca_V1.2$ or $Ca_V\alpha2\delta$) and the *green channel* (wheat germ agglutinin) are used to produce co-localization pixel maps using co-localization finder plugin. Co-localization is shown in *white* when the pixels for the *green* (wheat germ agglutinin) and the *red channels* (either $Ca_V1.2$ (*top*) or $Ca_V\alpha2\delta$ (*bottom*)) merge. Pearson's correlation coefficient were calculated from six cells using JACoP plugin (45). The Pearson's correlation coefficient values are expected to vary between +1 and −1, with +1 indicating a perfect correlation. The analysis was validated by further establishing that the Costes *p* value is 100% indicating that co-localization in the regions masked in *white* is highly probable. In this series of experiments, the Pearson's correlation coefficient values were 0.41 ± 0.03 (n = 6) for $Ca_V1.2$ and 0.72 ± 0.01 (n = 6) for $Ca_V\alpha2\delta$ indicating that both proteins are found at the plasma membrane in cultured cardiomyocytes.

expression was more important than the reduction in the total protein density. Altogether, these data suggest that the trafficking of $Ca_V\alpha2\delta$ was significantly disrupted by the double mutation. The decrease in the expression of $Ca_V\alpha2\delta$ caused a significant 40% reduction in the peak current density of $Ca_V1.2$ when co-expressed with $Ca_V\alpha2\delta$ WT in stable $Ca_V\beta3$ cells. Hence, the combination of two variants that are relatively silent polymorphisms on their own could significantly impair the trafficking of $Ca_V\alpha2\delta$ and consequently reduce L-type $Ca_V1.2$ currents.

Conclusion—Current genetic studies are placing the homeostasis of Ca^{2+} as a central modulator of cardiac repolarization with genes such as *CACNA1C* as well as *ATP2A2*, *PLN*, *PRKCA*, *SRL,* and *SLC8A1* (2). Genetic studies have reported a decreased expression of $Ca_V\alpha2\delta$ transcripts in patients suffering from atrial (43) and ventricular fibrillation (44). Our current results confirm that mutations in *CACNA2D1* could be a contributing factor in cardiac sudden death associated with a short QT interval. It is important to note that the strongest reduction in the cell surface density of $Ca_V\alpha2\delta$ was observed by combining two genetic variants that had little impact when tested individually. Hence, the role of polymorphisms in *CACNA2D1* is not to be neglected. Missense and/or truncation mutations of $Ca_V\alpha2\delta$ could severely impair $Ca_V1.2$ currents providing that the said mutation significantly decreases the cell surface protein expression of $Ca_V\alpha2\delta$.

Acknowledgments—We thank Serge Sénéchal and Dr. Jacques Thibodeau (Département de Microbiologie, Infectiologie et Immunologie, Université de Montréal, Montréal, Québec, Canada) for their help with the fluorescent-activated cell sorting experiments; Dr. Céline Fiset and Nabil El Khoury for providing protocols and assistance regarding mouse cardiomyocyte cell isolation and culture; Julie Verner for HEKT cell culture; Michel Brunette for technical assistance, and Louis Villeneuve for expert help with confocal microscopy.

REFERENCES

1. Roger, V. L., Go, A. S., Lloyd-Jones, D. M., Benjamin, E. J., Berry, J. D., Borden, W. B., Bravata, D. M., Dai, S., Ford, E. S., Fox, C. S., Fullerton, H. J., Gillespie, C., Hailpern, S. M., Heit, J. A., Howard, V. J., Kissela, B. M., Kittner, S. J., Lackland, D. T., Lichtman, J. H., Lisabeth, L. D., Makuc, D. M., Marcus, G. M., Marelli, A., Matchar, D. B., Moy, C. S., Mozaffarian, D., Mussolino, M. E., Nichol, G., Paynter, N. P., Soliman, E. Z., Sorlie, P. D., Sotoodehnia, N., Turan, T. N., Virani, S. S., Wong, N. D., Woo, D., and Turner, M. B. (2012) Heart disease and stroke statistics–2012 update: a report from the American Heart Association. *Circulation* **125,** e2–e220
2. Arking, D. E., Pulit, S. L., Crotti, L., van der Harst, P., Munroe, P. B., Koopmann, T. T., Sotoodehnia, N., Rossin, E. J., Morley, M., Wang, X., Johnson, A. D., Lundby, A., Gudbjartsson, D. F., Noseworthy, P. A., Eijgelsheim, M., Bradford, Y., Tarasov, K. V., Dörr, M., Müller-Nurasyid, M., Lahtinen, A. M., Nolte, I. M., Smith, A. V., Bis, J. C., Isaacs, A., Newhouse, S. J., Evans, D. S., Post, W. S., Waggott, D., Lyytikäinen, L. P., Hicks, A. A., Eisele, L., Ellinghaus, D., Hayward, C., Navarro, P., Ulivi, S., Tanaka, T., Tester, D. J., Chatel, S., Gustafsson, S., Kumari, M., Morris, R. W., Naluai, Å. T., Padmanabhan, S., Kluttig, A., Strohmer, B., Panayiotou, A. G., Torres, M., Knoflach, M., Hubacek, J. A., Slowikowski, K., Raychaudhuri, S., Kumar, R. D., Harris, T. B., Launer, L. J., Shuldiner, A. R., Alonso, A., Bader, J. S., Ehret, G., Huang, H., Kao, W. H., Strait, J. B., Macfarlane, P. W., Brown, M., Caulfield, M. J., Samani, N. J., Kronenberg, F., Willeit, J., Smith, J. G., Greiser, K. H., Meyer Zu, S. H., Werdan, K., Carella, M., Zelante, L., Heckbert, S. R., Psaty, B. M., Rotter, J. I., Kolcic, I., Polasek, O., Wright, A. F., Griffin, M., Daly, M. J., Arnar, D. O., Holm, H., Thorsteinsdottir, U., Denny, J. C., Roden, D. M., Zuvich, R. L., Emilsson, V., Plump, A. S., Larson, M. G., O'Donnell, C. J., Yin, X., Bobbo, M., D'Adamo, A. P., Iorio, A., Sinagra, G., Carracedo, A., Cummings, S. R., Nalls, M. A., Jula, A., Kontula, K. K., Marjamaa, A., Oikarinen, L., Perola, M., Porthan, K., Erbel, R., Hoffmann, P., Jockel, K. H., Kalsch, H., Nothen, M. M., den, H. M., Loos, R. J., Thelle, D. S., Gieger, C., Meitinger, T., Perz, S., Peters, A., Prucha, H., Sinner, M. F., Waldenberger, M., de Boer, R. A., Franke, L., van der Vleuten, P. A., Beckmann, B. M., Martens, E., Bardai, A., Hofman, N., Wilde, A. A., Behr, E. R., Dalageorgou, C., Giudicessi, J. R., Medeiros-Domingo, A., Barc, J., Kyndt, F., Probst, V., Ghidoni, A., Insolia, R., Hamilton, R. M., Scherer, S. W., Brandimarto, J., Margulies, K., Moravec, C. E., Fabiola, Fuchsberger, C., O'Connell, J. R., Lee, W. K., Watt, G. C., Campbell, H., Wild, S. H., El Mokhtari, N. E., Frey, N., Asselbergs, F. W., Leach,

I. M., Navis, G., van den Berg, M. P., van Veldhuisen, D. J., Kellis, M., Krijthe, B. P., Franco, O. H., Hofman, A., Kors, J. A., Uitterlinden, A. G., Witteman, J. C., Kedenko, L., Lamina, C., Oostra, B. A., Abecasis, G. R., Lakatta, E. G., Mulas, A., Orru, M., Schlessinger, D., Uda, M., Markus, M. R., Volker, U., Snieder, H., Spector, T. D., Arnlov, J., Lind, L., Sundstrom, J., Syvanen, A. C., Kivimaki, M., Kahonen, M., Mononen, N., Raitakari, O. T., Viikari, J. S., Adamkova, V., Kiechl, S., Brion, M., Nicolaides, A. N., Paulweber, B., Haerting, J., Dominiczak, A. F., Nyberg, F., Whincup, P. H., Hingorani, A. D., Schott, J. J., Bezzina, C. R., Ingelsson, E., Ferrucci, L., Gasparini, P., Wilson, J. F., Rudan, I., Franke, A., Muhleisen, T. W., Pramstaller, P. P., Lehtimaki, T. J., Paterson, A. D., Parsa, A., Liu, Y., van Duijn, C. M., Siscovick, D. S., Gudnason, V., Jamshidi, Y., Salomaa, V., Felix, S. B., Sanna, S., Ritchie, M. D., Stricker, B. H., Stefansson, K., Boyer, L. A., Cappola, T. P., Olsen, J. V., Lage, K., Schwartz, P. J., Kaab, S., Chakravarti, A., Ackerman, M. J., Pfeufer, A., de Bakker, P. I., and Newton-Cheh, C. (2014) Genetic association study of QT interval highlights role for calcium signaling pathways in myocardial repolarization. *Nat. Genet.* **46,** 826–836

3. Cerrone, M., Napolitano, C., and Priori, S. G. (2012) Genetics of ion-channel disorders. *Curr. Opin. Cardiol.* **27,** 242–252
4. Tester, D. J., and Ackerman, M. J. (2014) Genetics of long QT syndrome. *Methodist. Debakey. Cardiovasc. J.* **10,** 29–33
5. Napolitano, C., and Antzelevitch, C. (2011) Phenotypical manifestations of mutations in the genes encoding subunits of the cardiac voltage-dependent L-type calcium channel. *Circ. Res.* **108,** 607–618
6. Bodi, I., Mikala, G., Koch, S. E., Akhter, S. A., and Schwartz, A. (2005) The L-type calcium channel in the heart: the beat goes on. *J. Clin. Invest.* **115,** 3306–3317
7. Rosati, B., Dong, M., Cheng, L., Liou, S. R., Yan, Q., Park, J. Y., Shiang, E., Sanguinetti, M., Wang, H. S., and McKinnon, D. (2008) Evolution of ventricular myocyte electrophysiology. *Physiol. Genomics* **35,** 262–272
8. Györke, S., Hagen, B. M., Terentyev, D., and Lederer, W. J. (2007) Chain-reaction Ca signaling in the heart. *J. Clin. Invest.* **117,** 1758–1762
9. Seisenberger, C., Specht, V., Welling, A., Platzer, J., Pfeifer, A., Kühbandner, S., Striessnig, J., Klugbauer, N., Feil, R., and Hofmann, F. (2000) Functional embryonic cardiomyocytes after disruption of the L-type α_{1C} ($Ca_V1.2$) calcium channel gene in the mouse. *J. Biol. Chem.* **275,** 39193–39199
10. Rosati, B., Yan, Q., Lee, M. S., Liou, S. R., Ingalls, B., Foell, J., Kamp, T. J., and McKinnon, D. (2011) Robust L-type calcium current expression following heterozygous knockout of the Cav1.2 gene in adult mouse heart. *J. Physiol.* **589,** 3275–3288
11. Bers, D. M. (2002) Cardiac excitation-contraction coupling. *Nature* **415,** 198–205
12. Venetucci, L., Denegri, M., Napolitano, C., and Priori, S. G. (2012) Inherited calcium channelopathies in the pathophysiology of arrhythmias. *Nat. Rev. Cardiol.* **9,** 561–575
13. Catterall, W. A. (2000) Structure and regulation of voltage-gated Ca^{2+} channels. *Annu. Rev. Cell Dev. Biol.* **16,** 521–555
14. Peterson, B. Z., DeMaria, C. D., Adelman, J. P., and Yue, D. T. (1999) Calmodulin is the Ca^{2+} sensor for Ca^{2+}-dependent inactivation of L-type calcium channels. *Neuron* **22,** 549–558
15. Dolphin, A. C. (2009) Calcium channel diversity: multiple roles of calcium channel subunits. *Curr. Opin. Neurobiol.* **19,** 237–244
16. Dai, S., Hall, D. D., and Hell, J. W. (2009) Supramolecular assemblies and localized regulation of voltage-gated ion channels. *Physiol. Rev.* **89,** 411–452
17. Gao, T., Puri, T. S., Gerhardstein, B. L., Chien, A. J., Green, R. D., and Hosey, M. M. (1997) Identification and subcellular localization of the subunits of L-type calcium channels and adenylyl cyclase in cardiac myocytes. *J. Biol. Chem.* **272,** 19401–19407
18. Carl, S. L., Felix, K., Caswell, A. H., Brandt, N. R., Ball, W. J., Jr., Vaghy, P. L., Meissner, G., and Ferguson, D. G. (1995) Immunolocalization of sarcolemmal dihydropyridine receptor and sarcoplasmic reticular triadin and ryanodine receptor in rabbit ventricle and atrium. *J. Cell Biol.* **129,** 673–682
19. Bourdin, B., Marger, F., Wall-Lacelle, S., Schneider, T., Klein, H., Sauvé, R., and Parent, L. (2010) Molecular determinants of the Cavβ-induced plasma membrane targeting of the Cav1.2 channel. *J. Biol. Chem.* **285,** 22853–22863
20. Altier, C., Garcia-Caballero, A., Simms, B., You, H., Chen, L., Walcher, J., Tedford, H. W., Hermosilla, T., and Zamponi, G. W. (2011) The Cav[β] subunit prevents RFP2-mediated ubiquitination and proteasomal degradation of L-type channels. *Nat. Neurosci.* **14,** 173–180
21. Fuller-Bicer, G. A., Varadi, G., Koch, S. E., Ishii, M., Bodi, I., Kadeer, N., Muth, J. N., Mikala, G., Petrashevskaya, N. N., Jordan, M. A., Zhang, S. P., Qin, N., Flores, C. M., Isaacsohn, I., Varadi, M., Mori, Y., Jones, W. K., and Schwartz, A. (2009) Targeted disruption of the voltage-dependent calcium channel $\alpha2/\delta1$ subunit. *Am. J. Physiol. Heart Circ. Physiol.* **297,** H117–H124
22. Singer, D., Biel, M., Lotan, I., Flockerzi, V., Hofmann, F., and Dascal, N. (1991) The roles of the subunits in the function of the calcium channel. *Science* **253,** 1553–1557
23. Parent, L., Schneider, T., Moore, C. P., and Talwar, D. (1997) Subunit regulation of the humain brain α_{1E} calcium channel. *J. Membr. Biol.* **160,** 127–140
24. Splawski, I., Timothy, K. W., Sharpe, L. M., Decher, N., Kumar, P., Bloise, R., Napolitano, C., Schwartz, P. J., Joseph, R. M., Condouris, K., Tager-Flusberg, H., Priori, S. G., Sanguinetti, M. C., and Keating, M. T. (2004) Ca(V)1.2 calcium channel dysfunction causes a multisystem disorder including arrhythmia and autism. *Cell* **119,** 19–31
25. Splawski, I., Timothy, K. W., Decher, N., Kumar, P., Sachse, F. B., Beggs, A. H., Sanguinetti, M. C., and Keating, M. T. (2005) Severe arrhythmia disorder caused by cardiac L-type calcium channel mutations. *Proc. Natl. Acad. Sci. U.S.A.* **102,** 8089–8096
26. Gillis, J., Burashnikov, E., Antzelevitch, C., Blaser, S., Gross, G., Turner, L., Babul-Hirji, R., and Chitayat, D. (2012) Long QT, syndactyly, joint contractures, stroke and novel CACNA1C mutation: expanding the spectrum of Timothy syndrome. *Am. J. Med. Genet.* **158A,** 182–187
27. Raybaud, A., Dodier, Y., Bissonnette, P., Simoes, M., Bichet, D. G., Sauvé, R., and Parent, L. (2006) The role of the *GX*9*GX*3*G* motif in the gating of high voltage-activated Ca2+ channels. *J. Biol. Chem.* **281,** 39424–39436
28. Depil, K., Beyl, S., Stary-Weinzinger, A., Hohaus, A., Timin, E., and Hering, S. (2011) Timothy mutation disrupts the link between activation and inactivation in CaV1.2 protein. *J. Biol. Chem.* **286,** 31557–31564
29. Burashnikov, E., Pfeiffer, R., Barajas-Martinez, H., Delpón, E., Hu, D., Desai, M., Borggrefe, M., Häissaguerre, M., Kanter, R., Pollevick, G. D., Guerchicoff, A., Laiño, R., Marieb, M., Nademanee, K., Nam, G. B., Robles, R., Schimpf, R., Stapleton, D. D., Viskin, S., Winters, S., Wolpert, C., Zimmern, S., Veltmann, C., and Antzelevitch, C. (2010) Mutations in the cardiac L-type calcium channel associated with inherited J-wave syndromes and sudden cardiac death. *Heart Rhythm.* **7,** 1872–1882
30. Antzelevitch, C., Pollevick, G. D., Cordeiro, J. M., Casis, O., Sanguinetti, M. C., Aizawa, Y., Guerchicoff, A., Pfeiffer, R., Oliva, A., Wollnik, B., Gelber, P., Bonaros, E. P., Jr., Burashnikov, E., Wu, Y., Sargent, J. D., Schickel, S., Oberheiden, R., Bhatia, A., Hsu, L. F., Haïssaguerre, M., Schimpf, R., Borggrefe, M., and Wolpert, C. (2007) Loss-of-function mutations in the cardiac calcium channel underlie a new clinical entity characterized by ST-segment elevation, short QT intervals, and sudden cardiac death. *Circulation* **115,** 442–449
31. Templin, C., Ghadri, J. R., Rougier, J. S., Baumer, A., Kaplan, V., Albesa, M., Sticht, H., Rauch, A., Puleo, C., Hu, D., Barajas-Martinez, H., Antzelevitch, C., Lüscher, T. F., Abriel, H., and Duru, F. (2011) Identification of a novel loss-of-function calcium channel gene mutation in short QT syndrome (SQTS6). *Eur. Heart J.* **32,** 1077–1088
32. Wilde, A. A., and Ackerman, M. J. (2010) Exercise extreme caution when calling rare genetic variants novel arrhythmia syndrome susceptibility mutations. *Heart Rhythm* **7,** 1883–1885
33. Castellano, A., Wei, X., Birnbaumer, L., and Perez-Reyes, E. (1993) Cloning and expression of a third calcium channel β subunit. *J. Biol. Chem.* **268,** 3450–3455
34. Williams, M. E., Feldman, D. H., McCue, A. F., Brenner, R., Velicelebi, G., Ellis, S. B., and Harpold, M. M. (1992) Structure and functional expression of α_1, α_2, and β subunits of a novel human neuronal calcium channel subtype. *Neuron* **8,** 71–84
35. Shakeri, B., Bourdin, B., Demers-Giroux, P. O., Sauvé, R., and Parent, L.

(2012) A quartet of Leucine residues in the Guanylate Kinase domain of CaVbeta determines the plasma membrane density of the CaV2.3 channel. *J. Biol. Chem.* **287,** 32835–32847
36. Yasuda, T., Chen, L., Barr, W., McRory, J. E., Lewis, R. J., Adams, D. J., and Zamponi, G. W. (2004) Auxiliary subunit regulation of high voltage activated calcium channels expressed in mammalian cells. *Eur. J. Neurosci.* **20,** 1–13
37. Wall-Lacelle, S., Hossain, M. I., Sauvé, R., Blunck, R., and Parent, L. (2011) Double mutant cycle analysis identified a critical leucine residue in IIS4-S5 linker for the activation of the Cav2.3 calcium channel. *J. Biol. Chem.* **286,** 27197–27205
38. Yifrach, O., and MacKinnon, R. (2002) Energetics of pore opening in a voltage-gated K(+) channel. *Cell* **111,** 231–239
39. Cassidy, J. S., Ferron, L., Kadurin, I., Pratt, W. S., and Dolphin, A. C. (2014) Functional exofacially tagged N-type calcium channels elucidate the interaction with auxiliary $\alpha 2\delta 1$ subunits. *Proc. Natl. Acad. Sci. U.S.A.* **111,** 8979–8984
40. Platano, D., Qin, N., Noceti, F., Birnbaumer, L., Stefani, E., and Olcese, R. (2000) Expression of the $\alpha(2)\delta$ subunit interferes with prepulse facilitation in cardiac L-type calcium channels. *Biophys. J.* **78,** 2959–2972
41. Van Petegem, F., Duderstadt, K. E., Clark, K. A., Wang, M., and Minor, D. L., Jr. (2008) Alanine-scanning mutagenesis defines a conserved energetic hotspot in the Cavα1 AID-Cavβ interaction site that is critical for channel modulation. *Structure* **16,** 280–294
42. Cantí, C., Nieto-Rostro, M., Foucault, I., Heblich, F., Wratten, J., Richards, M. W., Hendrich, J., Douglas, L., Page, K. M., Davies, A., and Dolphin, A. C. (2005) The metal-ion-dependent adhesion site in the Von Willebrand factor-A domain of $\alpha 2\delta$ subunits is key to trafficking voltage-gated Ca^{2+} channels. *Proc. Natl. Acad. Sci. U.S.A.* **102,** 11230–11235
43. Gaborit, N., Steenman, M., Lamirault, G., Le Meur, N., Le Bouter, S., Lande, G., Léger, J., Charpentier, F., Christ, T., Dobrev, D., Escande, D., Nattel, S., and Demolombe, S. (2005) Human atrial ion channel and transporter subunit gene-expression remodeling associated with valvular heart disease and atrial fibrillation. *Circulation* **112,** 471–481
44. Sivagangabalan, G., Nazzari, H., Bignolais, O., Maguy, A., Naud, P., Farid, T., Massé, S., Gaborit, N., Varro, A., Nair, K., Backx, P., Vigmond, E., Nattel, S., Demolombe, S., and Nanthakumar, K. (2014) Regional ion channel gene expression heterogeneity and ventricular fibrillation dynamics in human hearts. *PLoS ONE* **9,** e82179
45. Bolte, S., and Cordelieres, F. P. (2006) A guided tour into subcellular colocalization analysis in light microscopy. *J. Microsc.* **224,** 213–232